JCEC
THE JOURNAL OF ENGINEERING AND EXACT SCIENCES

OPEN ACCESS

The Journal of Engineering and Exact Sciences – jCEC, Vol. 10 N. 05 (2024)
journal homepage: https://periodicos.ufv.br/jcec
eISSN: 2527-1075
ISSN: 2446-9416

Mechanical and Microstructural Analysis of Treated Tuff with Metakaolin Geopolymer Cement for Road Base layers Applications

Article Info:

Article history: Received 2024-05-05/ Accepted 2024-07-24 / Available online 2024-07-24

doi: 10.18540/jcecvl10iss5pp19363

Khadhra Allali
ORCID: https://orcid.org/0000-0002-3677-1638
FIMAS, Fiability of Materials and Structures in Saharian Regions Laboratory, Tahri Mohammed University, Bechar P.Box 417, Bechar 08000, Algeria
E-mail: allali.khadra@univ-bechar.dz

Nabil Bella
ORCID: https://orcid.org/0000-0003-3586-8304
FIMAS, Fiability of Materials and Structures in Saharian Regions Laboratory, Tahri Mohammed University, Bechar P.Box 417, Bechar 08000, Algeria
E-mail: bella.nabil@univ-bechar.dz

Abstract

Traditional road bases materials such as natural gravel and crushed stone are environmentally damaging, and there is a growing need for sustainable and eco-friendly alternatives. One such alternative is using geopolymer cement and tuff as aggregate materials. Geopolymer cement is an innovative and environmentally-friendly alternative to traditional Portland cement, and using locally-sourced tuff as an aggregate material can further reduce the environmental impact of road construction. This article discusses the importance of sustainable road construction practices, particularly in the use of eco-friendly materials for road base layers. It focuses on the treatment of tuff with alkali-activated metakaolin as the geopolymer precursor activated with a mixture of sodium hydroxide and sodium silicate. The effectiveness of treating tuff with metakaolin geopolymer cement is evaluated using several parameters, including dry density, California Bearing Ratio (CBR), shear strength, and microstructure analysis. These evaluations are performed with different NaOH dosages (8, 10, and 12 moles) to determine the optimal molarity for enhancing the material's performance.

Keywords: Road base layers. Geopolymer cement. Tuff. Kaolin. metakaolin geopolymer cement. shear strength

1. Introduction

Road base layers are an essential component of any road construction project, as they provide the necessary support and stability for the road surface. A well-designed and properly constructed road base layer can significantly improve the longevity and safety of a road. However, traditional road base materials such as natural gravel and crushed stone can be unsustainable and environmentally damaging (Gautam *et al*., 2018). There is a growing demand for sustainable and eco-friendly alternatives that can enhance the performance of road base layers while minimizing their environmental impact (Plati, 2019). This is where the use of sustainable materials such as geopolymer cement and tuff as aggregate materials comes in (Kantarcı *et al*., 2019) (Kantarci *et al*., 2021) (Amran *et al*., 2021). By using these materials, road builders can reduce the carbon footprint of their projects, while also improving the strength, durability, and longevity of the road base layers (Avirneni *et al*., 2016) (Tang *et al*., 2019) (N. B. Singh & Middendorf, 2020). The development of sustainable road construction practices is critical to reducing the impact of transportation on the environment, and using eco-friendly materials in road base layers is an important step in that direction (Jiang *et al*., 2018). Geopolymer cement is an innovative and eco-friendly substitute for traditional Portland cement (Okoye, 2017). It is made by reacting aluminosilicate materials, such as metakaolin, with alkaline activators to form a hard, durable binder (B. Singh *et al*., 2015). Geopolymer cement has demonstrated exceptional mechanical properties and is suitable for various applications, including road base layers (Hu *et al*., 2018). The use of geopolymer cement in road base layers has several potential benefits, such as improved strength, durability, and resistance to deformation (Kamal & Bas, 2021). Additionally, the use of locally-sourced materials, such as tuff, as aggregate in geopolymer cement mixtures can further reduce the environmental impact of road construction by reducing transportation costs and emissions. Tuff is a volcanic rock that is abundant in many regions (Germinario & Török, 2019), and it has been shown to have good physical and mechanical properties for use in road construction (Daheur *et al*., 2021). Utilizing geopolymer cement with tuff as an aggregate material allows for the creation of a sustainable and cost-effective road base layer capable of enduring heavy traffic loads and harsh environmental conditions. One method to enhance the properties of tuff is by treating it with metakaolin geopolymer cement. Metakaolin geopolymer cement is produced by combining metakaolin, an amorphous aluminosilicate material (calcined kaolin) , with an alkaline activator solution (Kamath *et al*., 2021). The resulting material is a highly durable and strong cement that can be used in various applications like the treatment of tuff (Chen *et al*., 2021). Kaolin is a clay mineral widely utilized in various industries such as ceramics, paper, paint, and cosmetics, among others (Majd *et al*., 2020). Algeria is a country that has significant reserves of kaolin, particularly in the eastern and central regions of the country. The kaolin deposits in Algeria are mainly found in the Aures and Hodna regions, as well as the Tlemcen and Mascara regions in the west (Boukoffa *et al*., 2021). The kaolin deposits in these regions are associated with various geological formations, including sedimentary rocks and volcanic rocks (AMRAOUI *et al*., 2022). The kaolin produced in Algeria is of high quality, characterized by high purity and low levels of impurities (Sahnoune *et al*., 2008). This makes it ideal for a variety of industrial uses, such as the production of high-quality ceramics, paper, and paint. Tabelbela Kaolin is a type of kaolin mineral that is found in the Tabelbela region of the Bechar Province in southwestern Algeria. The Tabelbela Kaolin deposits are located in the foothills of the

Saharan Atlas Mountains, and are associated with Cretaceous sedimentary rocks (Zenasni *et al*., 2014). Tabelbela Kaolin is known for its high purity and brightness, with a white color that makes it suitable for various industrial applications (Rikioui *et al*., 2021). The kaolin deposits in the Tabelbela region are considered to be among the highest quality kaolin deposits in Algeria, with a high degree of whiteness, low levels of impurities, and excellent rheological properties (Nabbou *et al*., 2019).

Currently, the trend in research is to utilize local materials to minimize project costs. In light of this, we have undertaken a study to enhance the value of an available local resource (Tabelbela Kaolin) by incorporating it into the foundation of road pavements. This study focuses on the methodology of treating tuff with metakaolin geopolymer cement studying several parameters. These include dry density, California Bearing Ratio (CBR), shear strength, and microstructure analysis. Generally, investigating the effects of treating tuff with metakaolin geopolymer cement can offer valuable insights into the potential applications of this material in construction and infrastructure.

2. Materials and Methods

2.1 Materials

2.1.1. Tuff:

The Tuff used is from SARL PRODAG200 company BECHAR ALGERIA., its mineral nature is silico-calcareous, and it is largely used in pavement base layers and embankments in Bechar (Fig. 1).

Figure 1 - Tuff

The grain size distribution according to NF P94-056 is shown in Figure 2. Based on the GTR 2000 Soil Classification (Gtr, 2000) , used Tuff belongs to the B5 class. It is characterized as sandy and gravelly soil with very silty fines. It is also sensitive to variations in moisture content and have relatively high permeability, considered stable but requiring reinforcement measures for use in road and other structure construction. Therefore, treating this tuff with metakaolin geopolymer cement is crucial. Based on the X-ray analyses summarized in Table 1, it appears that the used tuff is a type of calcareous tuff, which contains substantial amounts of calcium oxide (CaO) and carbon dioxide (CO_2). The presence of CaO suggests that the tuff is composed of calcium-rich minerals, such as calcite ($CaCO_3$) or aragonite ($CaCO_3$), which are commonly found in limestone and other sedimentary rocks (Tiago & Gil, 2020). The high percentage of SiO_2 (silica) and Al_2O_3 (alumina) suggests that the tuff also contains significant amounts of volcanic ash or other pyroclastic materials, which may have been deposited along with the calcium-rich minerals during volcanic activity (Levitskii *et al*., 2013). Overall, the chemical

composition suggests that the tuff is a calcareous volcanic rock, which consists of a blend of calcium-rich minerals and volcanic ash or other pyroclastic materials.

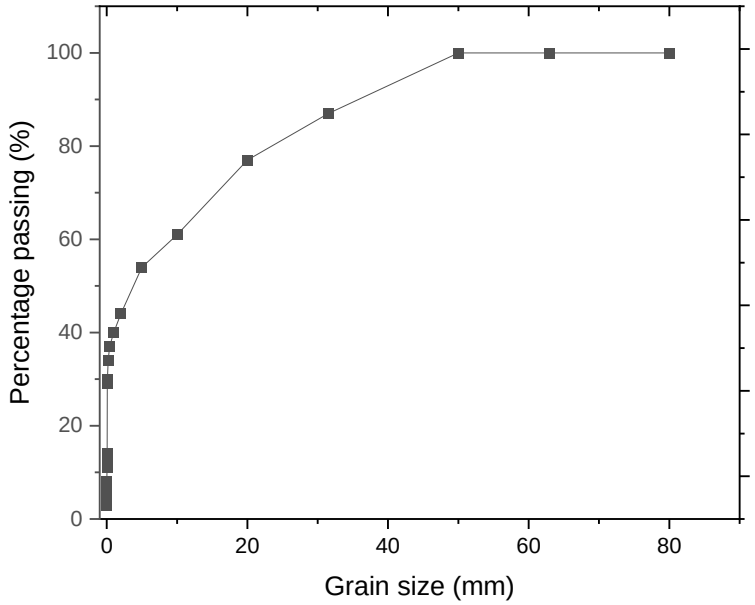

Figure 2 - Particle size distribution of Tuff

Table 1 - X-ray analyses of Tuff.

CaO	CO_2	SiO_2	Al_2O_3	Fe_2O_3	MgO	K_2O	Sc_2O_3	SO_3	TiO_2	Cl	Others
44.65%	31.4 %	16.44%	4.65%	1.44%	0.88%	0.43%	0.36%	0.23%	0.20%	0.05%	0.11%

2.1.2. Kaolin:

Used kaolin is from deposit at Tabelbala belongs to the Ugarta Mountains (400 km in the east of Bechar ALGERIA), it is also referred to as the Makhlouf deposit, due to its proximity to Makhlouf village. (Fig. 3).

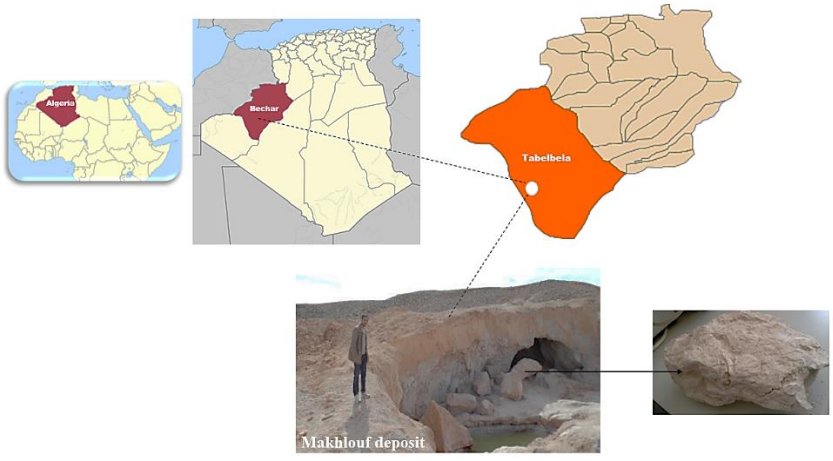

Figure 3 - Kaolin of Tabelbela

Grain size distribution according to NF P 94-057 is shown in Figure 4. According to the GTR 2000 Soil Classification (Gtr, 2000) , kaolin is classified as an A2 type soil. The soils of category A2 are

fine soils such as clays, silts, and clayey silts that are characterized as impermeable, unstable, and have low bearing capacity. Based on the chemical analysis presented in Table 2, our kaolin is a type of clay mineral that is primarily composed of silicon dioxide (SiO_2) and aluminum oxide (Al_2O_3). Kaolinite is the most common mineral in kaolin, and it has a chemical formula of $Al_2Si_2O_5(OH)_4$ (Hamzaoui *et al*., 2015). The high percentage of SiO_2 and Al_2O_3 indicates that the given kaolin has a high degree of purity, which makes it suitable for various industrial applications, including ceramics, papermaking, and paint production (Khalifa *et al*., 2020). The relatively low percentage of Fe_2O_3 (iron oxide) suggests that kaolin has a low level of impurities, which also makes it suitable for high-quality applications. The presence of CO_2 in the kaolin may suggest the inclusion of some organic matter, which is not unusual for kaolin The organic matter may have been incorporated into the kaolin during its formation or may have been introduced through environmental factors such as soil or groundwater (Wang & Mulligan, 2006). Overall, the chemical composition suggests that kaolin is a high-quality, pure clay mineral that is suitable for a range of industrial applications.

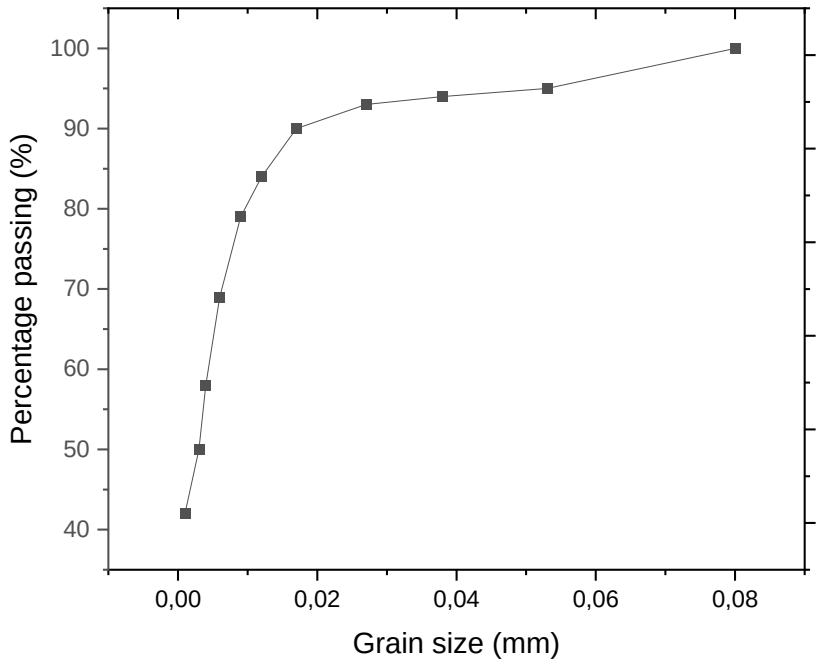

Figure 4 - Particle size distribution of Tabelbela Kaolin

Table 2 - X-ray analyses of Kaolin.

SiO_2	Al_2O_3	CO_2	Fe_2O_3	K_2O	TiO_2	SO3	MgO	CaO	BaO	SrO	Others
52.99%	31.88%	4.9%	4.81%	2.13%	1.62%	0.92%	0.52%	0.41%	0.13%	0.07%	0.17%

2.1.3. Activator:

The activator used was a solution comprising water glass, sodium hydroxide, and water. Used

Water Glass was from SIGMA-ALDRICH, its formula is Na2(SiO2), xH2O, with a density equal to 1,390, PH: 11,7. Sodium hydroxide NaOH was from commercial store its purity is 99% (Fig. 5). The water utilized for mixing is sourced from the potable water supply of the city, which originates from the "Djorftorba" dam located at a distance of 6km from Bechar town.

Waterglass NaOH

Figure 5 - Alkaline activator

2.2 Laboratory techniques

All tests were conducted in LTPO / Western Public Works Laboratory (Physical-chemical tests, Modified Proctor compaction test, California Bearing Ratio test (CBR)) and the laboratory of technology at the Tahri Mohammed University of Bechar, Algeria (Direct shear test).

2.2.1. Characterization of materials

The physical and chemical characteristics of Kaolin (K) and Tuff (T), such as Grain size distribution analysis (particle size distribution), Specific gravity, Atterberg limits (liquid limit, plastic limit, and plasticity index), Chemical analysis, methylene blue (MB), Bulk and absolute density, are determined according to European and French test standards.

2.2.2. Modified Proctor compaction test

The compaction tests were conducted in compliance with NF P94-093 standards. This test employs compaction force to determine the relationship between moisture content and dry density and identifies the dry density of the material and its corresponding moisture level, which is referred to as the Optimal Moisture Content (OMC). The sample material is dried in an oven and then divided into four equal parts before being mixed with a specified amount of water to ensure even distribution. The resulting mixture is then placed in a mold and compacted with an automatic compactor for 55 strokes. The moisture content of the sample is then measured, and the process is repeated with varying amounts of water until an optimal point is reached, generating a curve that illustrates the relationship between dry density and moisture content. Accordingly, different mixtures composed of treated tuff with Metakaolin Geopolymer Cement (MKGPC) and varying dosages of NaOH (8, 10, and 12 moles) were compacted at different moisture contents. This was done to estimate the OMC and the Maximum Dry Density (MDD) using the modified Proctor test, as indicated in Table 3.

Table 3 - Composition of treated Tuff with MKGPC.

Compounds (g)	8 moles	10 moles	12 moles
Metakaolin (MK)	220	220	220
Water (total)	220	220	220
NaOH	52.15	69.75	87.35
WG	170.38	170.38	170.38
W/MK	1	1	1
W_{WG}	110	110	110
W_{mix}	110	110	110
Tuff	5280	5280	5280

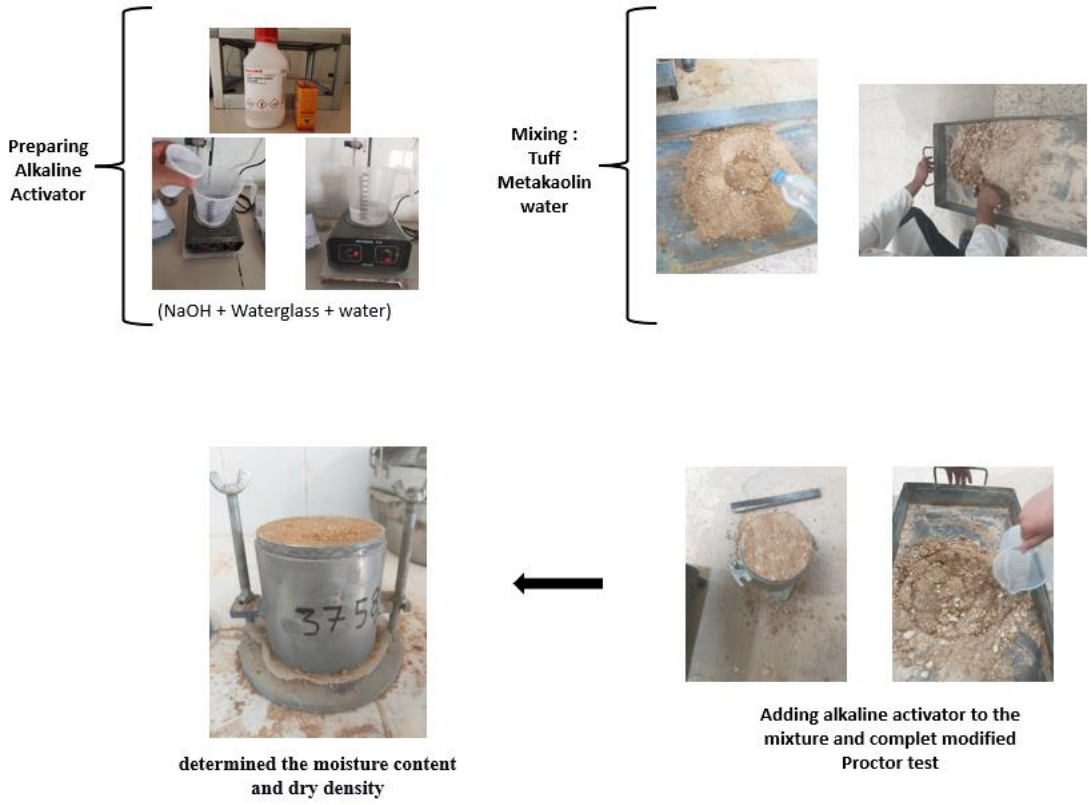

Figure 6 - Modified Proctor test

2.2.3. California Bearing Ratio test (CBR)

To perform the CBR test, a cylindrical sample measuring 177.8 mm in height and 152.4 mm in diameter is prepared using the Proctor method, with an optimum moisture content based on the NF P94-078 standard. Next, a penetration test is conducted using a cylindrical piston with a diameter of 50 mm, maintaining a consistent penetration rate of 1.27 mm/min. The CBR index is calculated by determining the percentage of pressure exerted by the piston on the bottom of the sample at a specific penetration

force level. This test aims to assess the soil's capacity to withstand traffic loads, thereby determining the necessary thickness for pavement foundation layers. The test involves creating test specimens using the CBR mold with a compaction energy of 55 blows per layer and at water contents corresponding to the optimum level determined in the modified Proctor test, where CBR is determined immediately after compaction.

Figure 7 - CBR test

2.2.4. Direct shear

The direct shear test, being the most ancient and uncomplicated form of shear testing, is frequently employed for assessing soil shear strength due to its quick testing time and straightforward sample preparation (Thiha *et al*., 2018).The direct shear tests were conducted using an automated SHEARMATIC EmS direct/residual shear testing apparatus (an advanced version of the conventional direct shear test apparatus). During the test, a constant normal load is applied to the upper half of the shear box, while the lower half is pushed horizontally, causing the sample to shear along the interface plane (Liu *et al*., 2005). The setup, which includes the direct shear box and the data acquisition system, is depicted in Figure 8, providing an overall perspective.

Figure 8 - SHEARMATIC apparatus

All mixtures of treated tuff with metakaolin geopolymer cement, using NaOH dosages of 8, 10, and 12 moles, were statically compacted at the Proctor optimum before being placed in the direct shear box. Every mixture of every dosage of NaOH was repeated at different ages of curing (1,7 and 28 days) under ambient temperature (20°C to 27°C). The test mode involves a rapid speed of 1 mm/min, consistent with an unconsolidated undrained (UU) test as per the standard NF P 94-071-1. This configuration is employed to assess the effect of geopolymer treatment on soil cohesion (c) and friction angle (ϕ). The applied normal stresses were 100, 300, and 600 kPa. Mohr-Coulomb failure envelopes for both untreated and treated samples were plotted by identifying the normal and shear stresses at failure.

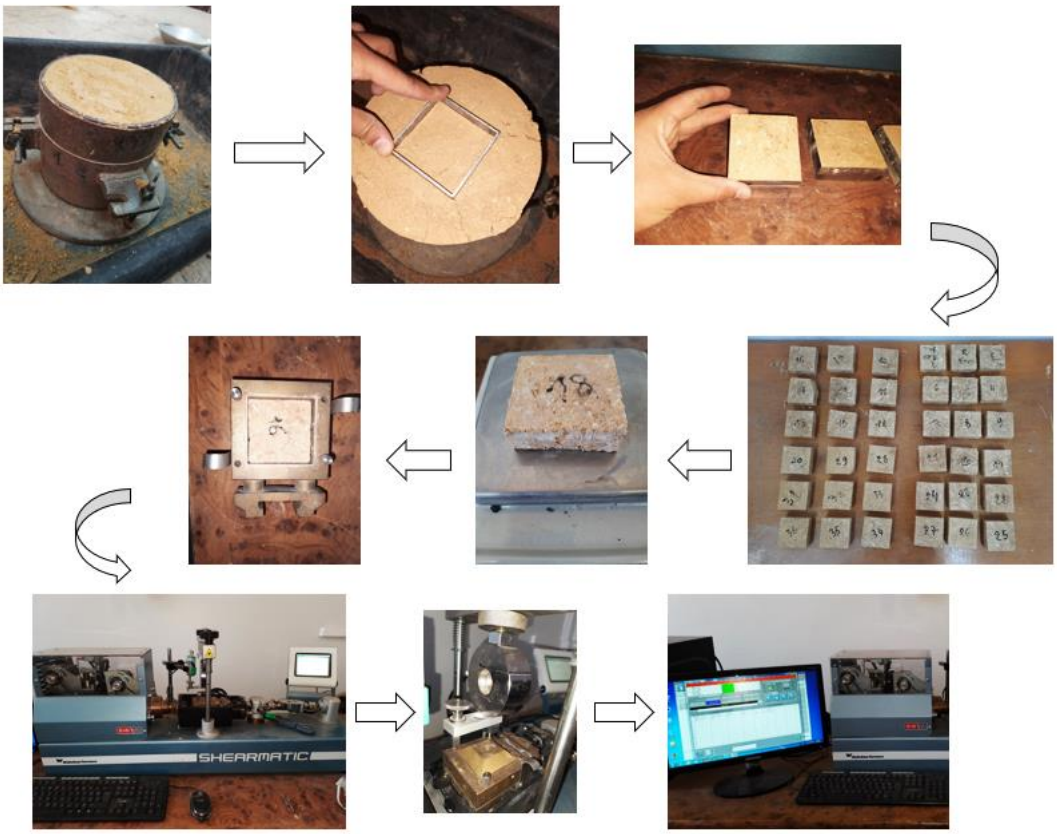

Figure 9 - Direct shear test

2.2.5. Microstructure analysis

2.2.5.1. Geopolymer synthesis

Metakaolin is widely used as a raw material for geopolymer synthesis. Here are the basic steps for synthesizing a metakaolin-based geopolymer:

1 - Preparation of raw materials: First Kaolin was milled using microgrinder machine and we sift it through 125 µm sieve, then Kaolin was burned using Muffle furnace at temperature of 650 °C during 1h to obtain Metakaolin. The alkaline activator solution is prepared by mixing sodium hydroxide (NaOH) at different concentrations (8, 10, and 12 moles) with water glass (Na2(SiO2)) and water to achieve a specific concentration.

2 - Mixing of raw materials: The dried metakaolin powder is blended with the alkaline activator solution in a specific ratio, followed by the addition of the untreated tuff. The mixing carried out by using a mortar and pestle to ensure that the mixture is homogenous.

3 - Formation of geopolymer gel: The mixture is stirred or mixed vigorously to ensure complete mixing. The mixture subsequently begins to form a geopolymer gel as a result of the reaction between the metakaolin and the alkaline activator solution.

4 - Dryness: The geopolymer gel is then dried at an ambient temperature for a specific duration of time. The drying process is carried out at a temperature of 37-40°C for 24-48 hours to ensure the geopolymer gel hardens and forms a solid material with high mechanical strength.

5 - Microstructure analysis: XRD was used to identify the crystalline phases and amorphous content, while SEM provided insights into the microstructure. EDX analysis was conducted to identify the elemental composition. Microstructure analysis (XRD, SEM) involves examining the treated tuff material under a microscope to determine the structure and composition of the material at a microscopic level. Analyzing the microstructure of treated tuff allows for assessing the effectiveness of metakaolin geopolymer cement treatment in altering the internal structure of the tuff material, enhancing its properties, and increasing its durability.

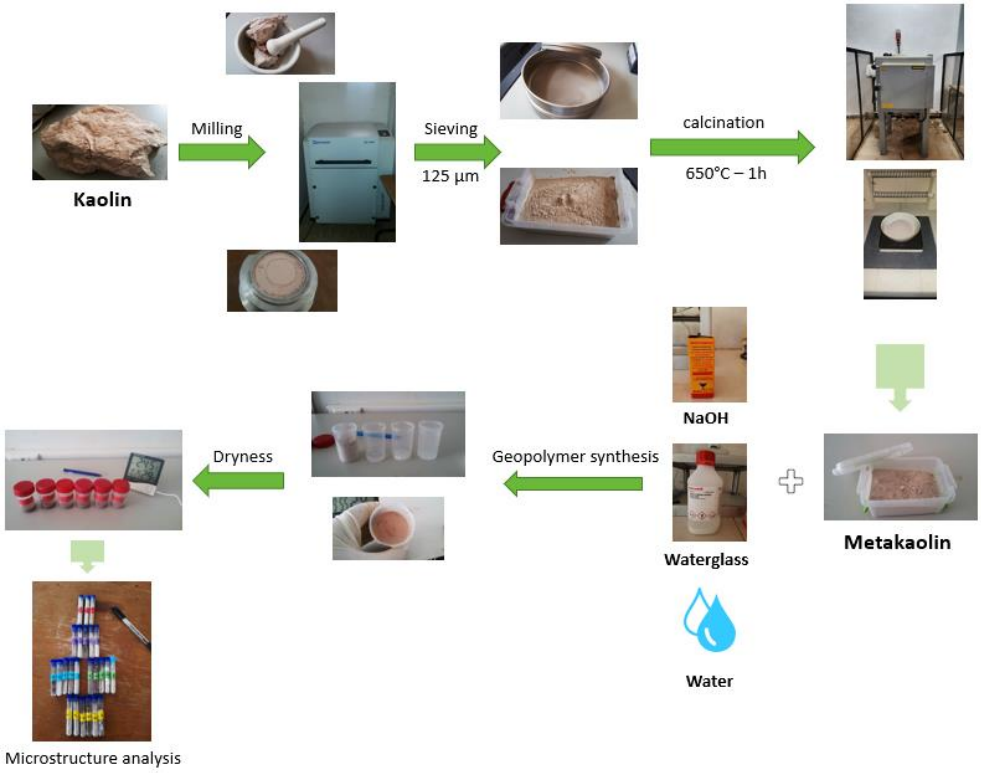

Figure 10 - Metakaolin geopolymer cement synthesis

2.2.5.2. X-Ray Diffraction (XRD)

XRD is a primary non-destructive method used to examine the crystalline structures in composite materials, which is crucial as various crystal phases result in distinct material properties. Understanding this aspect in-depth is therefore critical. Bragg's law, which describes the relationship between the angles of coherent and incoherent scattering in a lattice ($\lambda = 2d \sin \theta$), is fundamental to XRD. This method can be applied not only to crystalline substances but also to amorphous materials, such as certain polymers and biomolecules, by using a small angular range of approximately 0.1-3 degrees (Polini & Yang, 2017).

2.2.5.3. Scanning electron microscopy (SEM)

SEM is a technique that provides detailed information about the microstructure of a coating surface, including the distribution of photocatalysts on the substrate, as well as the uniformity and morphology of particles within the coating. By analyzing cross-sectional images, one can obtain valuable information regarding the thickness and uniformity of the coating. Additionally, backscatter detection can produce elemental composition mapping images, which offer insight into the distribution

of species and the separation, dispersion, and percolation processes occurring between the photocatalytic coatings and substrates (Faraldos & Bahamonde, 2018).

The microstructure analysis was done on Physical-Chemical Analysis Platform (PTAPC) CRAPC, Laghouat, Algeria.

3. Results and discussion

3.1 Characterization of materials

The geotechnical properties of Kaolin (K) and Tuff (T) as determined from the basic laboratory testing are summarized in Table 4.

Table 4 - Geotechnical properties of K and T.

Geotechnical properties	kaolin	Tuff	Test standards
Bulk density (g/cm^3)	1.98	2.32	NF EN 1936
Absolute density(g/cm^3)	-	2.56	//
liquid limit (Wl) (%)	44.5	26	NF P94-051
plastic limit (Wp) (%)	26.9	18.7	//
plasticity index (PI) (-)	17.9	7.3	//
methylene blue (MB)	2.11	0.25	NF EN 933-9
Carbonate $CaCO_3$ (%)	2.8	68.2	NF P 15-461
Sulfate SO_4^{-2}(%)	0.41	-	//
Chloride Cl- (%)	0.14	0.11	//
InsolublesSiO2-MgO-AL2O3-CaO-Fe2O(%)	96.65	31.69	//

(-) dimension less quantity

3.2 Modified compaction test

The results of the modified compaction test for the studied mixtures are presented in Figure 11. For reference, the maximum dry density of Untreated Tuff (UT) was 2.04 g/cm³, with an optimum moisture content of 8%. A similar-shaped compaction curve is observed for treated Tuff with metakaolin geopolymer cement (TTG) using 8, 10, and 12 mol NaOH, with an optimum moisture content of 8.16% (considering the water in the alkaline activator). The significantly higher dry density value in the case of TTG compared to UT highlights the stabilizing effect of metakaolin geopolymer cement. The maximum dry density of 2.13 g/cm³ (TTG with 12 moles of NaOH) is notably higher than the maximum achieved for the other tested mixtures.

The MKGPC treated Tuff had an approximately 4% higher MDD than the untreated Tuff. The increase in dry density can be attributed to the filling of the pores in the tuff by the metakaolin geopolymer cement, resulting in a denser material. As the NaOH concentration increases, the dissolution of tuff particles progresses, making the particles less angular and easier to compact, which leads to an increase in density (Yu *et al*., 2023).

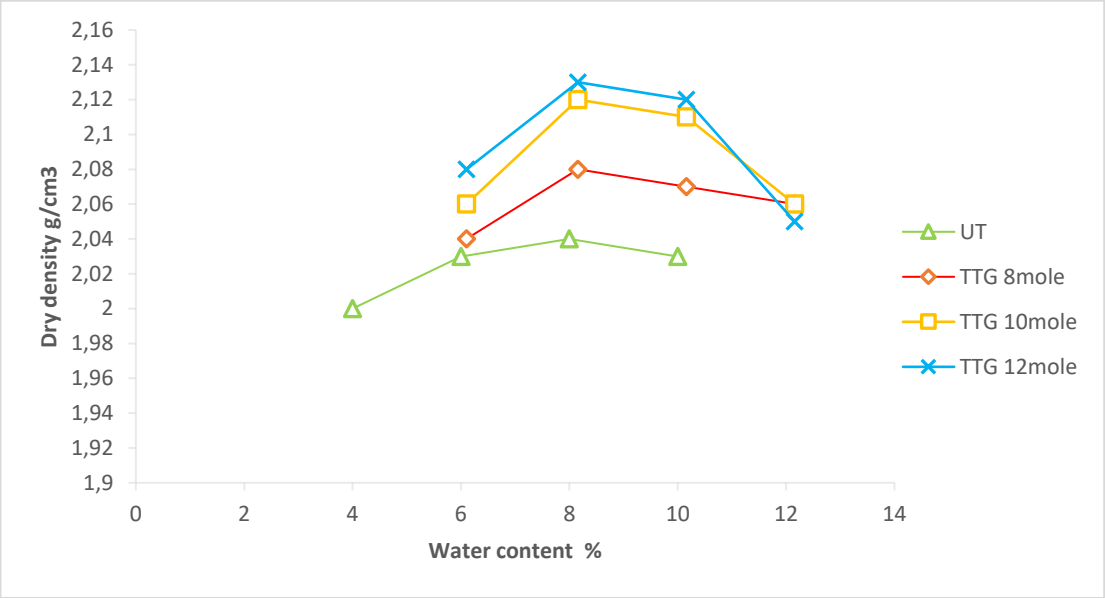

Figure 11 - Modified Proctor curve

3.3 California Bearing Ratio test

Figure 12 shows the histograms from the 95% Optimum moisture content CBR test on the mixtures. As a reference point, UG demonstrates a CBR of 124. In every instance, the CBR index values exceed 80%, meeting the requirement set by the CEBTP (CEBTP, 1984) for granular materials to be considered suitable as a foundation layer for flexible pavements. The CBR index decreases as the dosage of NaOH in the TTGs mixture increases, declining from 119% to 98% to 91% for TTG concentrations of 8, 10, and 12 moles, respectively. However, if the NaOH concentration becomes excessively high, the final product may experience depolymerization, resulting in a decrease in the amount of binders (Yu *et al*., 2023). As reported by Zangana (Bahaadin Noory Zangana, 2012), in all cases where sodium hydroxide was applied, there was an observed peak in CBR at an optimal dosage, which then diminished with higher concentrations. These findings run counter to the trends observed in the Modified Proctor test's optimal dry densities (as shown in Figure 11). Typically, higher dry densities lead to a more compact and densely packed material characterized by reduced pore space and increased particle interlocking. Consequently, this can restrict particle mobility and deformation under load, ultimately resulting in a decreased CBR index.

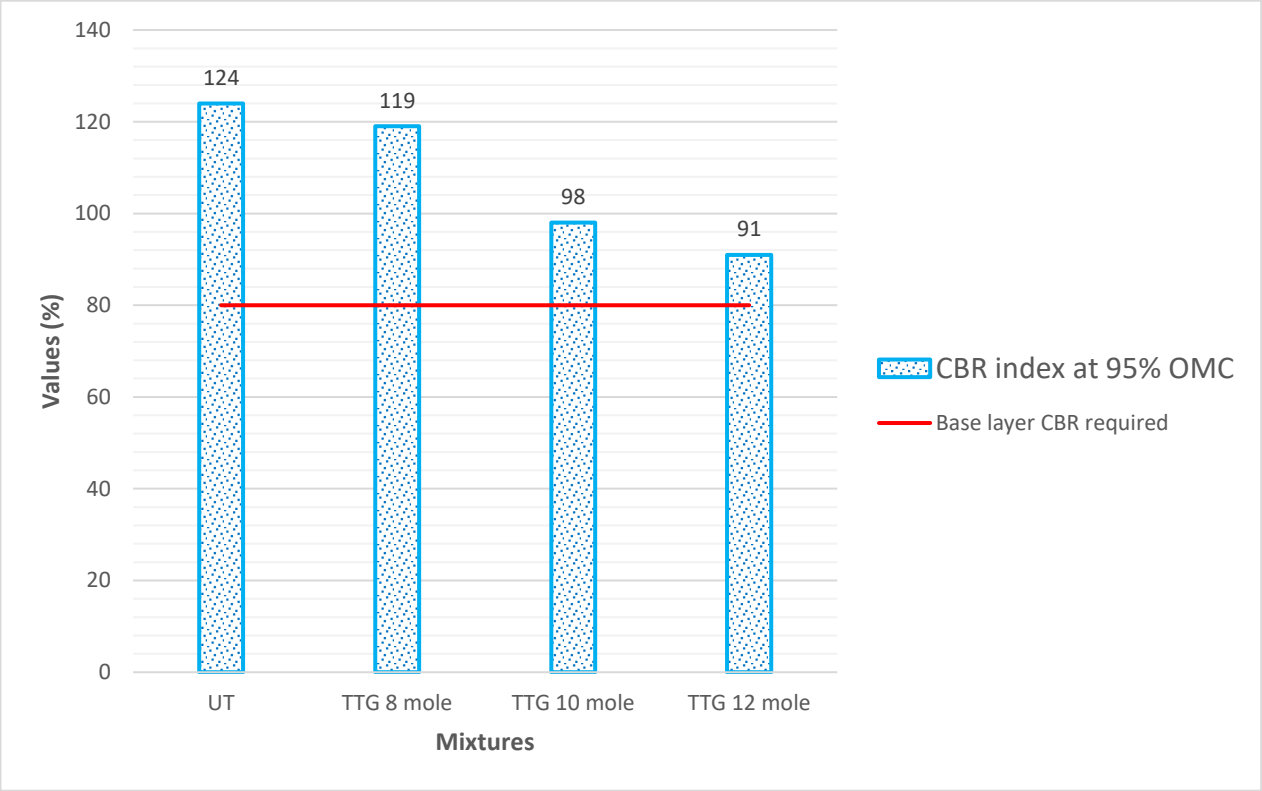

Figure 12 -Variation of the CBR index at 95% OPM of the mixtures

3.4 Direct shear

Based on the field test results, Figure 13 illustrates the horizontal shear stress–horizontal displacement curves and the vertical displacement–horizontal displacement curves for the direct shear tests of UT and TTG's under different normal stress conditions at various curing ages (1, 7, and 28 days). Figure 14 presents the Mohr-Coulomb envelope derived from the direct shear test results of UT and TTG's, detailing the shear strength parameters: cohesion (c) and friction angle (ϕ).

(a)

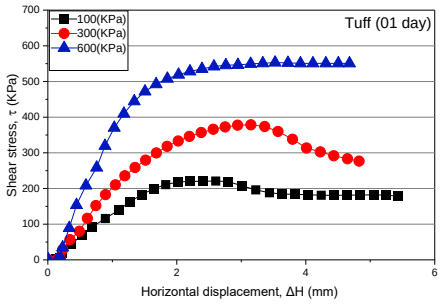
Tuff (01 day)
100(KPa)
300(KPa)
600(KPa)
Shear stress, τ (KPa)
Horizontal displacement, ΔH (mm)

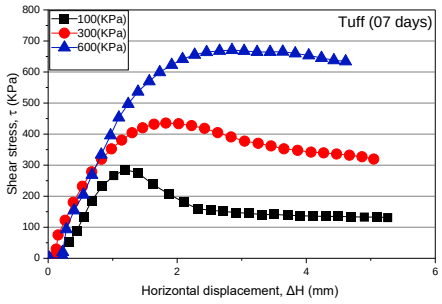
Tuff (07 days)
100(KPa)
300(KPa)
600(KPa)
Shear stress, τ (KPa)
Horizontal displacement, ΔH (mm)

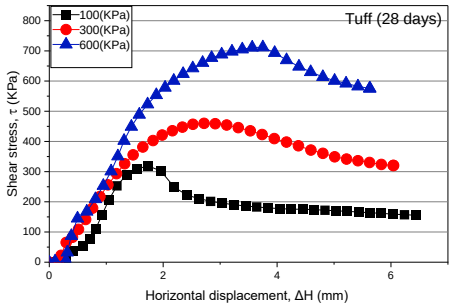
Tuff (28 days)
100(KPa)
300(KPa)
600(KPa)
Shear stress, τ (KPa)
Horizontal displacement, ΔH (mm)

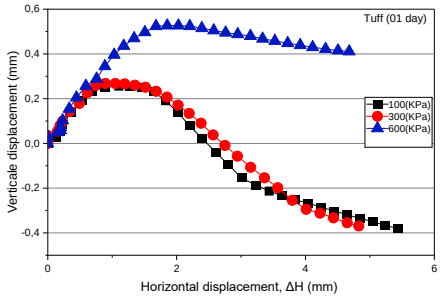
Tuff (01 day)
100(KPa)
300(KPa)
600(KPa)
Verticale displacement (mm)
Horizontal displacement, ΔH (mm)

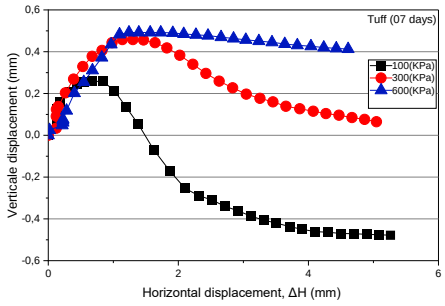
Tuff (07 days)
100(KPa)
300(KPa)
600(KPa)
Verticale displacement (mm)
Horizontal displacement, ΔH (mm)

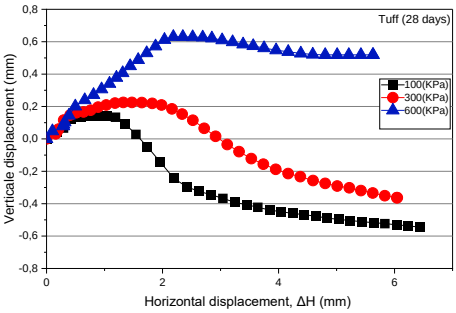
Tuff (28 days)
100(KPa)
300(KPa)
600(KPa)
Verticale displacement (mm)
Horizontal displacement, ΔH (mm)

(b)

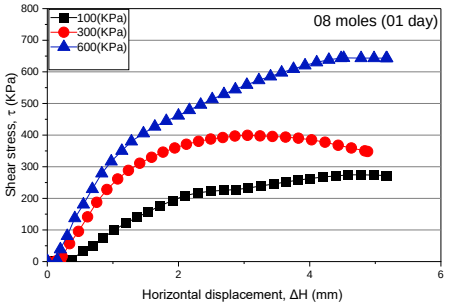
08 moles (01 day)
100(KPa)
300(KPa)
600(KPa)
Shear stress, τ (KPa)
Horizontal displacement, ΔH (mm)

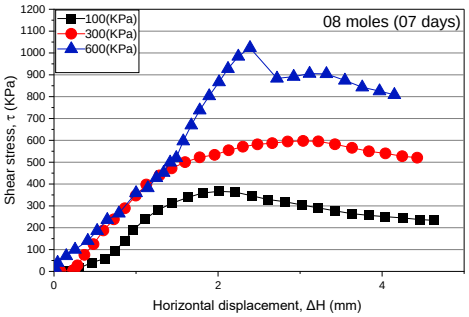
08 moles (07 days)
100(KPa)
300(KPa)
600(KPa)
Shear stress, τ (KPa)
Horizontal displacement, ΔH (mm)

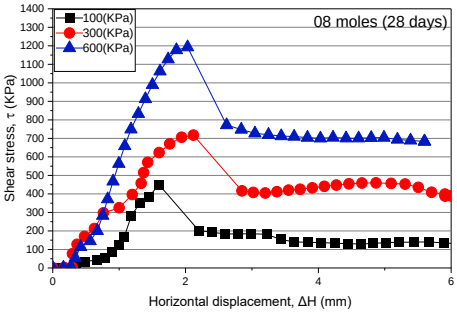
08 moles (28 days)
100(KPa)
300(KPa)
600(KPa)
Shear stress, τ (KPa)
Horizontal displacement, ΔH (mm)

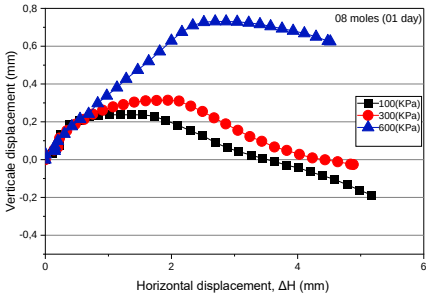
08 moles (01 day)
100(KPa)
300(KPa)
600(KPa)
Verticale displacement (mm)
Horizontal displacement, ΔH (mm)

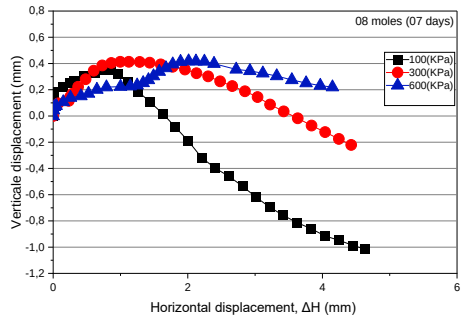
08 moles (07 days)
100(KPa)
300(KPa)
600(KPa)
Verticale displacement (mm)
Horizontal displacement, ΔH (mm)

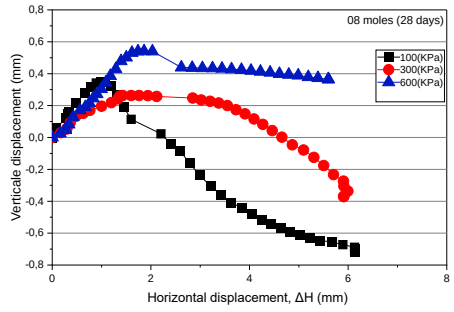
08 moles (28 days)
100(KPa)
300(KPa)
600(KPa)
Verticale displacement (mm)
Horizontal displacement, ΔH (mm)

(c)

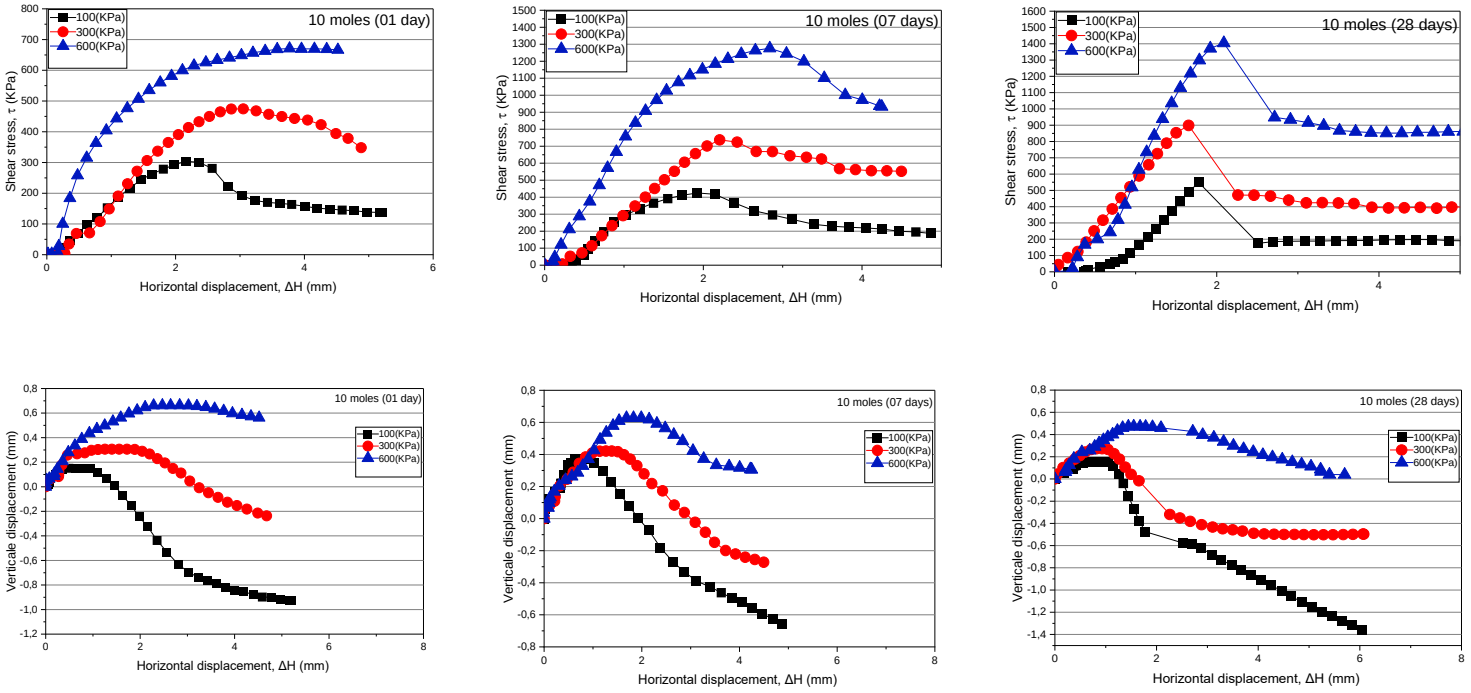

(d)

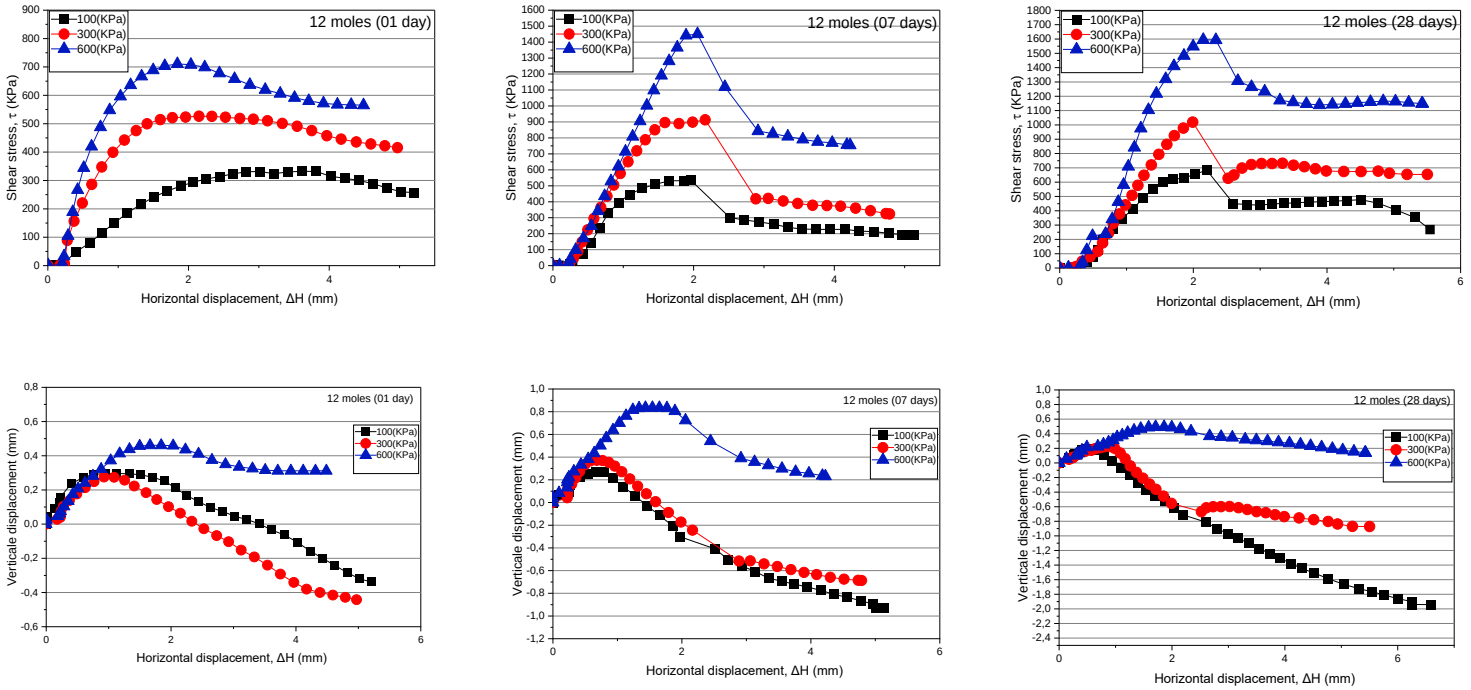

Figure 13 - Result curves of direct shear tests: (a) UT, (b) TTG 8mole, (c) TTG 10mole, (d) TTG 12mole

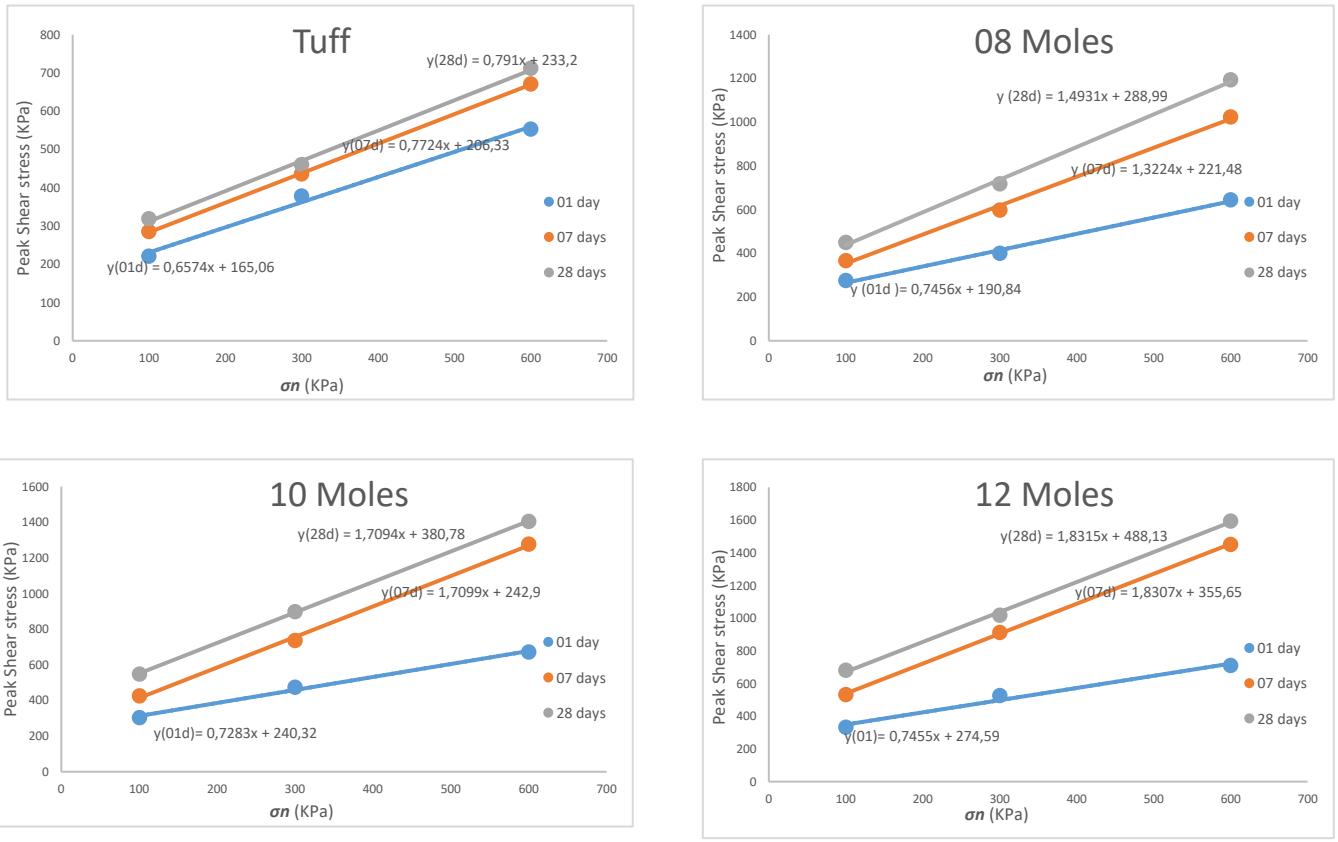

Figure 14 - The relationship curves between shear strength and normal stress of UT and TTG's

From Figures 13 and 14, we observe the following:

(1) As the normal stress increases, the shear strength of both untreated tuff (UT) and tuff treated with geopolymer cement (TTG) also increases gradually. The proportion of NaOH in the TTG's significantly affects its shear strength. Under identical normal stress conditions, the shear strength of TTG increases with higher NaOH proportions.

(2) From the shear stress–horizontal displacement curve, TTG's give higher strengths in shearing than UT and those higher strengths increase more in all soil types through curing state. the Direct Shear Strength (DSS) of UT, TTG 8moles, TTG 10moles and TTG 12moles estimated 712.056, 1192.72, 1404.29 and 1594.33KPa for 28 days under normal stress of 600 KPa, respectively. Upon compaction with a metakaolin-based geopolymer, the Tuff gradually harden over time as a chemical reaction takes place between the soil particles and geopolymer molecules (Thiha *et al.*, 2018).

(3) Analyzing the vertical displacement versus horizontal displacement curves, we find that under lower normal stress, both UT and TTG exhibit dilatant behavior before reaching a stable state. The shear dilatation value increases with the proportion of NaOH. As normal stress increases, both UT and TTG undergo an extended shear dilatation phase. Subsequently, as shear displacement progresses, they transition to a shear shrinking phase and eventually reach a stable state. The shear strength parameters of the TTG's were much greater than that of the UT. The

average cohesion values obtained in the direct shear test were enhanced from 233.1974 kPa for UT to 288.9936, 380.7813, and 488,1275 kPa for the TTG 8moles, TTG 10moles, and TTG 12moles, respectively (28 days of curing) . Although the Tuff is normally low internal friction angle, the compacted condition with metakaolin geopolymer cement makes a higher internal friction angle. The average friction angle of the UT was 38.1939°, whereas that of the TTG 8moles, TTG 10moles, and TTG 12moles ranged from 56.04762, 59.7025 and 61.2682°, respectively (28 days of curing). The advancement of geopolymers has led to higher shear strength measurements in soils treated with geopolymers such as NASHgel and CASHgel. This is achieved through the activation of soil and fly ash components by alkalis, which results in increased contact between soil particles, ultimately improving shear strength parameters (Hamid & Alnuaim, 2023).

(4) The findings from the direct shear test indicate that the shear strength parameters of the TTG samples were notably superior to those of the UT samples. The highest values for cohesion and friction angle were observed in the TTG with a concentration of 12 moles of NaOH. However, the microstructure analysis (XRD, SEM, EDX) must be conducted to determine the appropriate dosage.

3.5 Microstructure analysis

3.5.1. X-Ray Diffraction (XRD):

Figure 15 shows the XRD patterns of the kaolin, metakaolin, Metakaolin geopolymer cement (MKGPM) 8,10 and 12mole, Tuff and Tuff with Metakaolin geopolymer cement (TuffMKGPM) 8,10 and 12mole. According to the XRD pattern, Kaolin shows peaks for kaolinite (K), quartz (Q), and halloysite (H). Kaolin typically shows peaks corresponding to kaolinite (a clay mineral), which is a layered silicate mineral. When kaolin is thermally treated (calcined), it transforms into metakaolin. The XRD pattern of metakaolin shows a reduction in the intensity of kaolinite peaks and the appearance of amorphous silica and alumina phases, indicating the breakdown of the kaolin structure.

The XRD analysis of the MKGPM samples reveals distinct patterns based on the molarity of the alkaline activator used. For the 8mole sample, the XRD pattern shows significant residual crystalline phases, including kaolinite and quartz, indicating incomplete geopolymerization. In contrast, the 10mole sample demonstrates optimal transformation, with fewer residual crystalline phases and a more pronounced amorphous hump, suggesting better geopolymerization and a well-developed aluminosilicate network. The 12mole sample shows a further reduction in crystalline phases, indicating an even more complete geopolymerization process. However, it also raises concerns about potential excess alkali issues, which could impact the long-term durability of the material.

The XRD analysis of tuff and TuffMKGPM samples provides comprehensive insights into their crystalline structures. Tuff, a volcanic ash rock composed of various minerals, prominently shows peaks for quartz (Q) and calcite (C) in its XRD pattern, reflecting its mineral composition. When tuff is added to MKGPM, the XRD pattern reveals a combination of tuff and geopolymer phases. This is evident as the peaks corresponding to quartz and calcite from the tuff remain, while new amorphous phases characteristic of the geopolymer emerge.

For the TuffMKGPM samples:

- The 8 mole TuffMKGPM sample exhibits higher residual crystalline phases, indicating incomplete geopolymerization.
- The 10 mole TuffMKGPM sample demonstrates a balanced phase transformation with fewer residual crystalline phases, suggesting a more effective geopolymerization process.
- The 12 mole TuffMKGPM sample displays minimal residual crystalline phases, indicating a nearly complete geopolymerization. However, there are potential concerns regarding excess alkali content, which could affect the material's long-term stability.

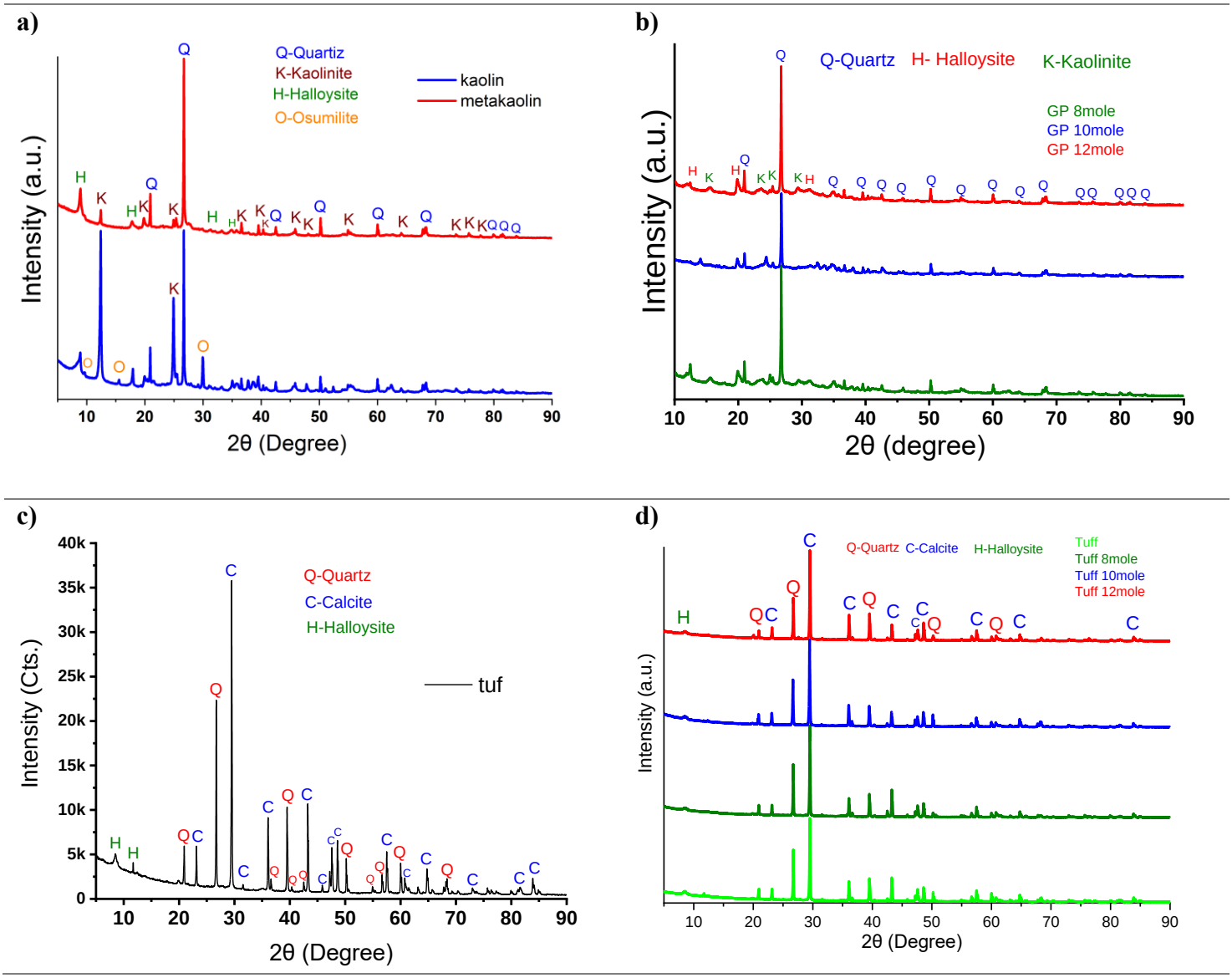

Figure 15 - The XRD patterns of a) kaolin and metakaolin, b) MKGPM 8,10 and 12mole , c) Tuff , d) TuffMKGPM 8,10 and 12mole

3.5.2. Scanning Electron Microscopy (SEM) and Energy-Dispersive X-ray Spectroscopy (EDX):

Figures 16 ,17 and 18 display representative microstructural regions observed by SEM, along with the chemical characterization results by EDX for both kaolin and metakaolin, Metakaolin geopolymer cement (MKGPM) 8,10 and 12mole, Tuff and Tuff with Metakaolin geopolymer cement (TuffMKGPM)

8,10 and 12mole. For kaolin and metakaolin, SEM images revealed two essential structures in kaolin: an agglomeration of thin layers with thicknesses ranging from 97 to 108 nm, and larger particles ranging from 389.19 nm to 1 μm in diameter. Metakaolin, subjected to thermal treatment, displayed three essential structures: an agglomeration of thin layers around 200 nm, larger particles ranging from 1 to 2 μm in diameter, and small shrapnel with diameters ranging from 80 to 200 nm. The shrapnel likely resulted from the thermal treatment of kaolin at 650°C to convert it into metakaolin. The EDX spectra for these materials showed elemental peaks for silicon (Si), aluminum (Al), and oxygen (O), reflecting their fundamental composition.

In the case of Metakaolin Geopolymer Cement (MKGPM), the SEM images depicted a dense, homogenous matrix with fewer voids as the molar concentration increased. The 8 mole geopolymer exhibited a cauliflower-like structure with an internal nanostructure of fine grains around 97 nm. The 10 mole geopolymer showed an internal structure of fine grains, but the general shape appeared as large, rock-like formations around 2 μm. Similarly, the 12 mole geopolymer displayed an internal structure of fine grains with a general shape resembling large rocks, consistent with the 10mole sample. The EDX spectra of MKGPM samples indicated the chemical composition of the geopolymer matrix, with peaks for Si, Al, and additional elements introduced during the geopolymerization process.

For tuff and TuffMKGPM, SEM images showed that tuff has a porous, granular structure with shrapnel ranging from 65 to 100 nm in diameter. When combined with MKGPM, the SEM images depicted how the geopolymer matrix encapsulates the tuff particles, resulting in a composite structure. The EDX spectra indicated the presence of elements from both tuff (such as Si, Al, and Ca from calcite) and the geopolymer matrix.

The SEM images of TuffMKGPM samples revealed three essential structures:

- Shrapnel from the tuff structure, selected by the blue line.
- Geopolymer-related structures, selected by the black line.
- A random large phase attributed to the basic structure of the tuff, selected by the red line.

This was observed in all molarities (8, 10, and 12 moles), with the 12mole sample showing a greater proportion of the random large phase, possibly due to the increased molar ratio of the geopolymer.

After comparing the mechanical and microstructural analyses, we can conclude that the 10mole mixture demonstrated higher compressive strength compared to the 8mole mixture, attributed to more complete geopolymerization and a denser microstructure. The 12mole mixture, while showing the highest compressive strength, raised concerns about brittleness and potential microcracking. The values for cohesion and friction angle were higher in the 10mole mixture, indicating better bonding and stability, whereas the 8mole mixture, while still showing adequate performance, had lower values in these parameters. The 12mole mixture exhibited high values but with potential durability issues. The 10 mole TuffMKGPM sample demonstrated a balance between complete geopolymerization and minimal residual crystalline phases, as evidenced by XRD. SEM images revealed a dense and homogenous microstructure with minimal voids, suggesting superior mechanical integrity. EDX analysis confirmed uniform elemental distribution, indicative of optimal chemical reactions during geopolymerization. In contrast, the 8mole sample showed incomplete geopolymerization, and the 12mole sample, while

showing extensive phase transformation, exhibited potential microcracking issues. In our previous study (ALLALI *et al*., 2024), we observed that the unconfined compressive strength (UCS) of gravel treated with Metakaolin geopolymer (TGG) was higher than that of gravel treated with cement (TGC). The optimal NaOH concentration was found to be 8 moles, which resulted in the highest UCS of 3.9 MPa. Comparatively, TGG with 10 moles NaOH gave a UCS of 3.57 MPa, and TGG with 12 moles NaOH achieved a UCS of 3.45 MPa after 90 days of curing. In the current study, the appropriate molarity was determined to be 10 moles, underscoring the importance of microstructure analysis using XRD and SEM to confirm mechanical results. The variation in results between the two studies can be attributed to the different materials used: the first study involved untreated gravel, whereas the second utilized untreated tuff. These differences in material characteristics likely influenced the interaction with metakaolin geopolymer cement, highlighting the need for thorough microstructural analysis to understand the underlying reasons for the observed mechanical properties.

(a)

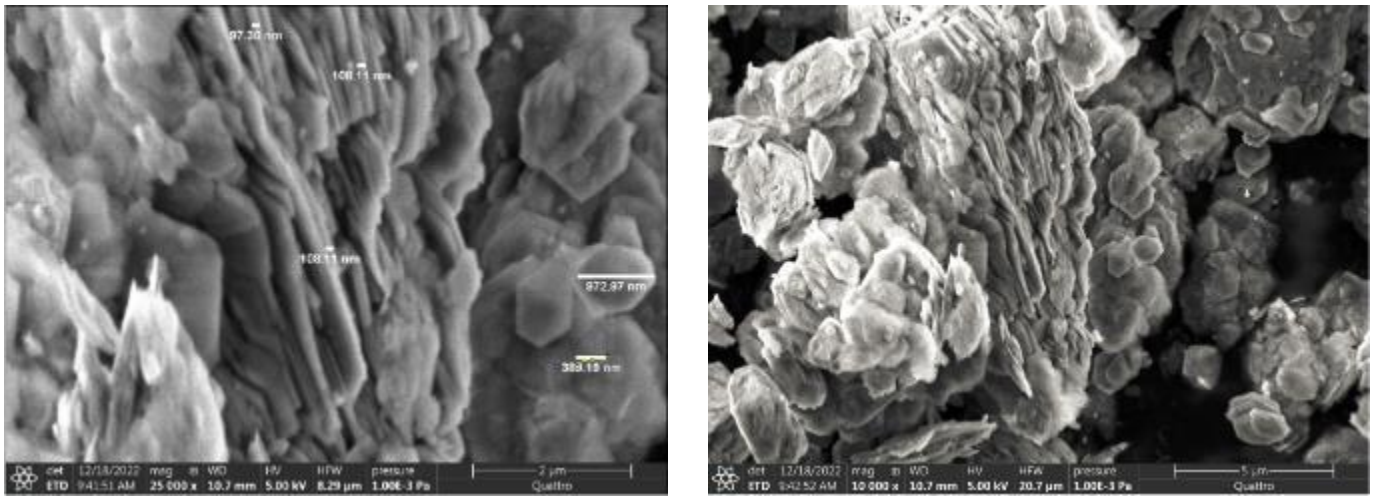

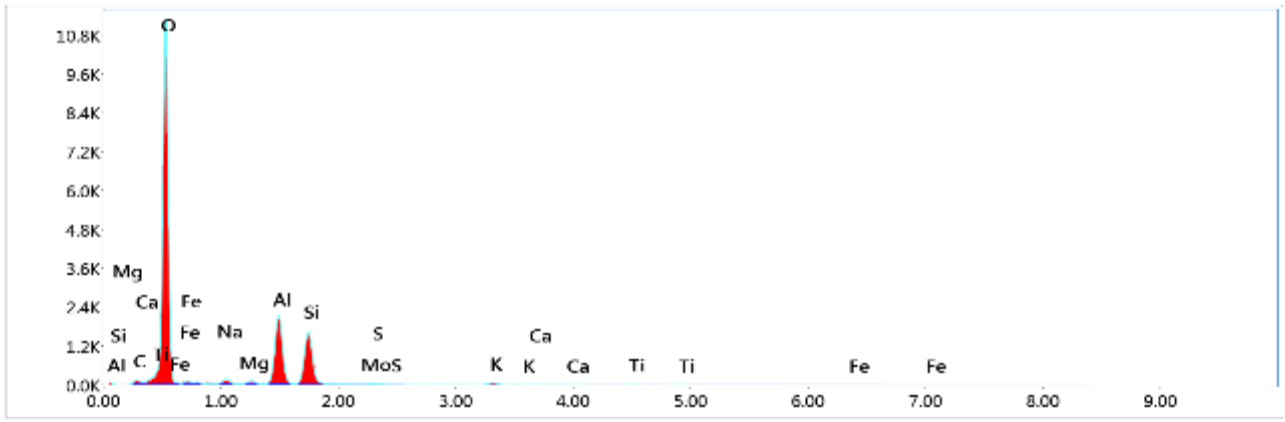

(b)

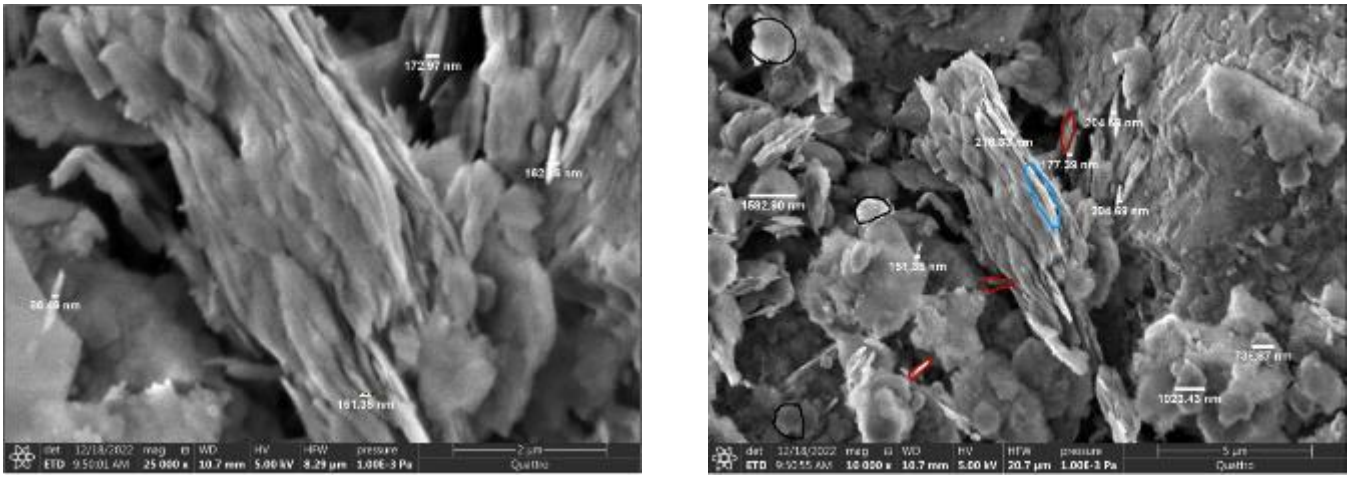

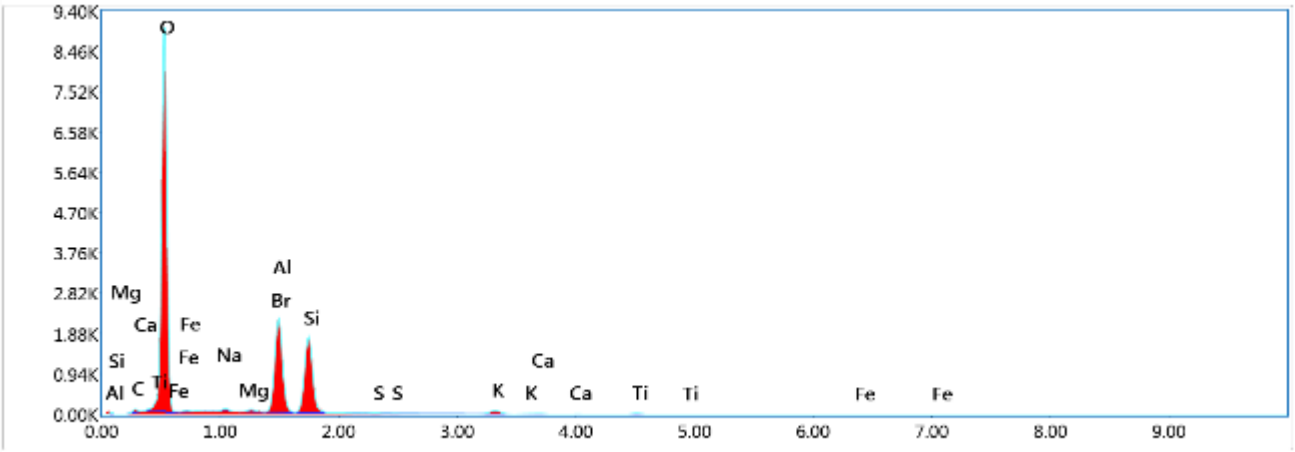

Figure 16 - SEM micrographs and SEM-EDX spectra (a) kaolin, (b) metakaolin

(a)

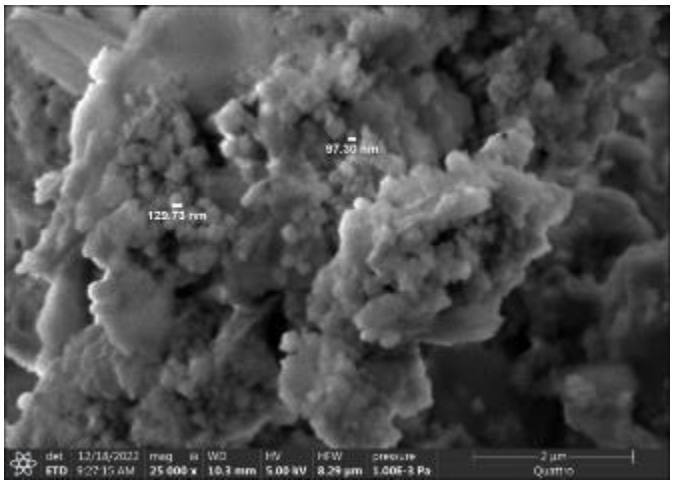
97.50 nm
129.73 nm

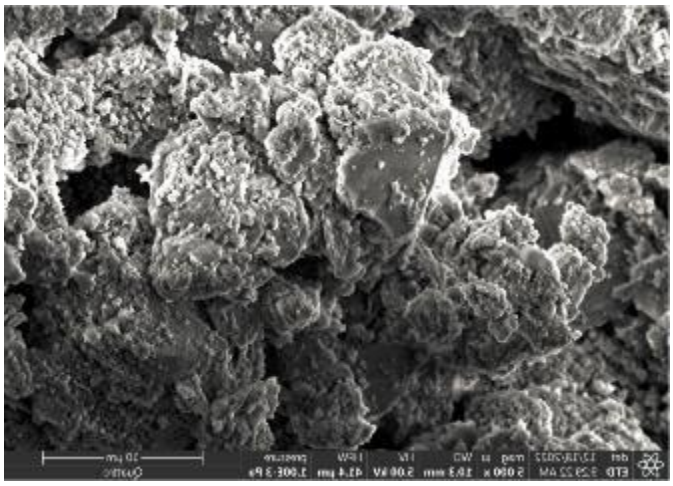

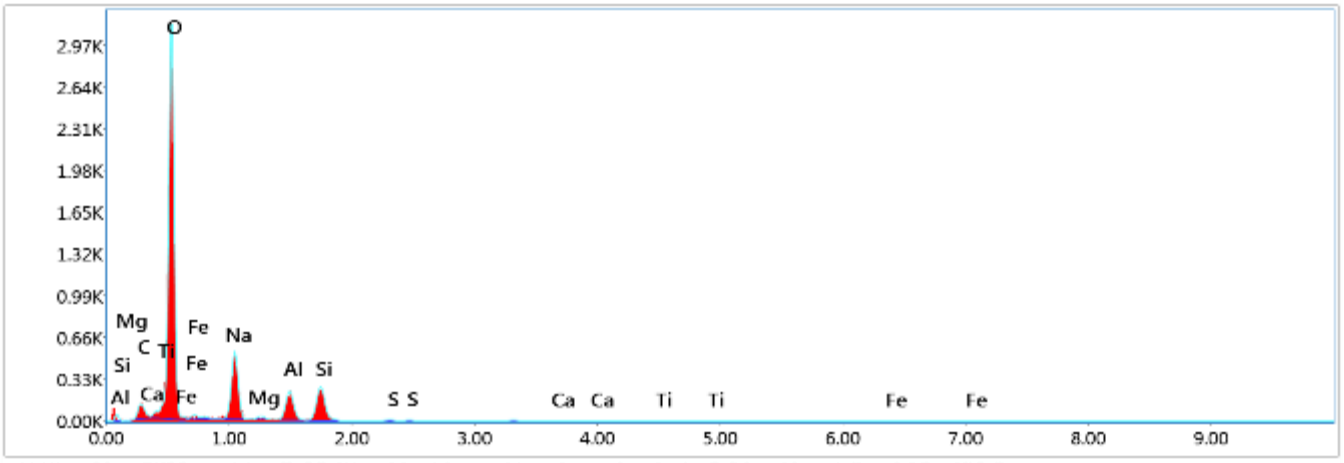
2.97K
2.64K
2.31K
1.98K
1.65K
1.32K
0.99K
0.66K
0.33K
0.00K
0.00
1.00
2.00
3.00
4.00
5.00
6.00
7.00
8.00
9.00
O
Mg
Si
Al
C
Ca
Ti
Fe
Fe
Fe
Na
Mg
Al
Si
S S
Ca Ca
Ti Ti
Fe
Fe

(b)

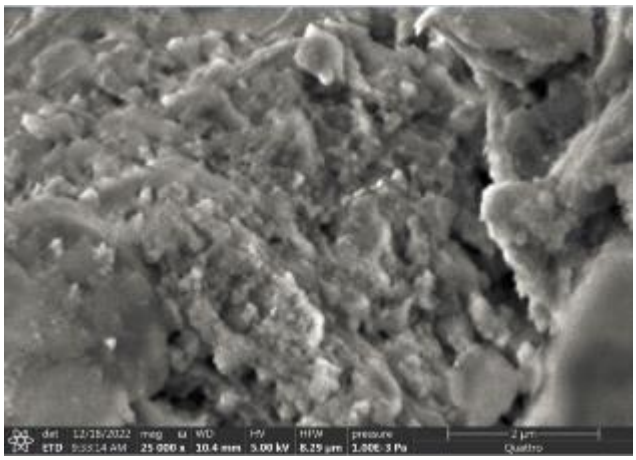

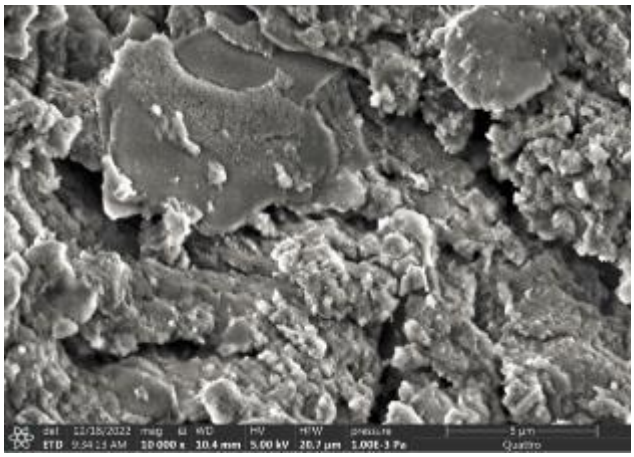

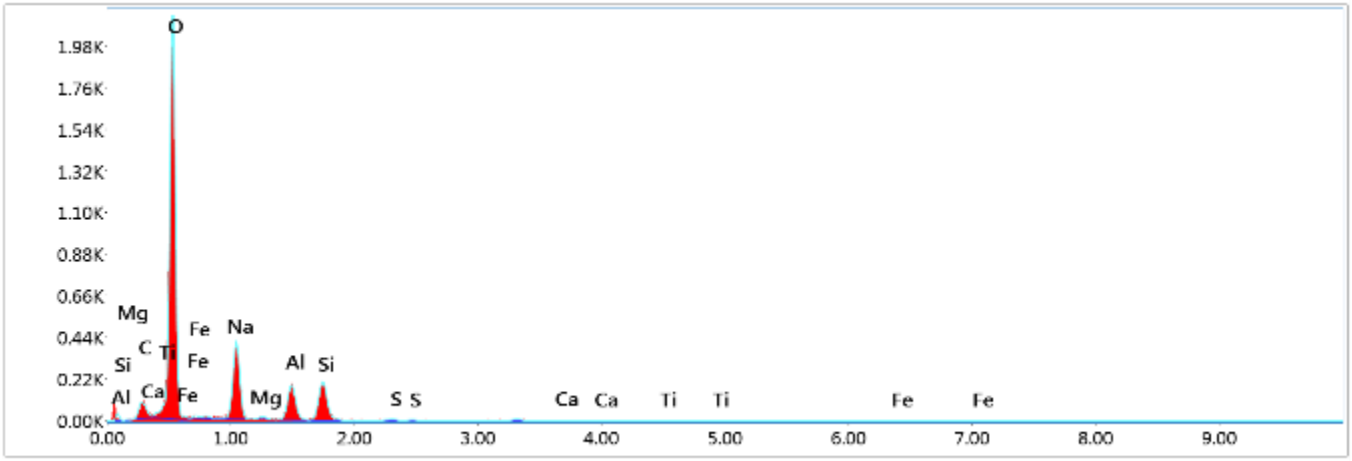
1.98K
1.76K
1.54K
1.32K
1.10K
0.88K
0.66K
0.44K
0.22K
0.00K
O
Mg
Si
C
Ti
Al
Ca
Fe
Fe
Fe
Na
Mg
Al
Si
S S
Ca Ca
Ti Ti
Fe
Fe
0.00
1.00
2.00
3.00
4.00
5.00
6.00
7.00
8.00
9.00

(c)

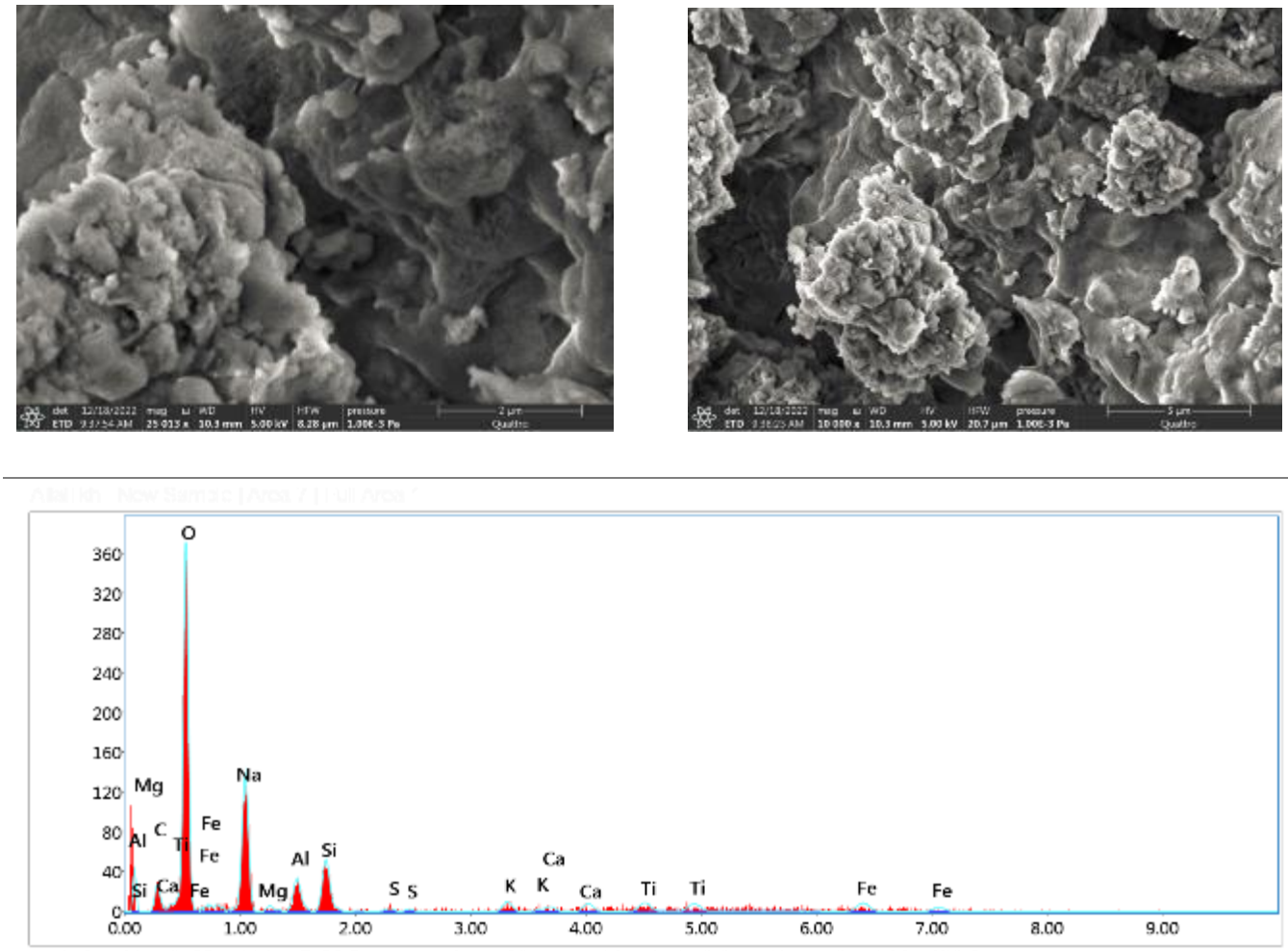

Figure 17 - SEM micrographs and SEM-EDX spectra (a) MKGPM 8mole, (b) MKGPM 10mole, (c) MKGPM 12mole

(a)

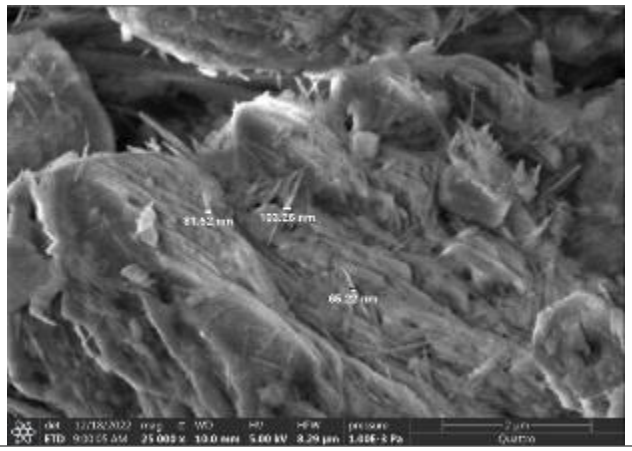

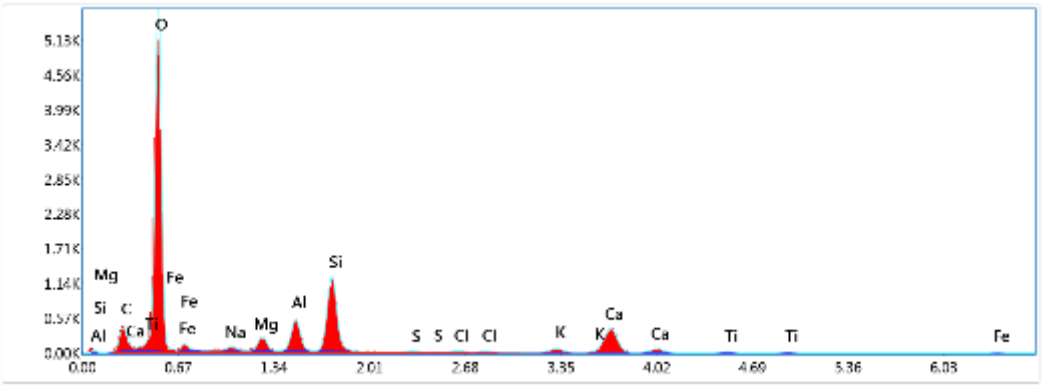
O
Mg
Si
C
Al
Ca
Ti
Fe
Fe
Fe
Na
Mg
Al
Si
S
S
Cl
Cl
K
K
Ca
Ca
Ti
Ti
Fe
5.13K
4.56K
3.99K
3.42K
2.85K
2.28K
1.71K
1.14K
0.57K
0.00K
0.00
0.67
1.34
2.01
2.68
3.35
4.02
4.69
5.36
6.03

(b)

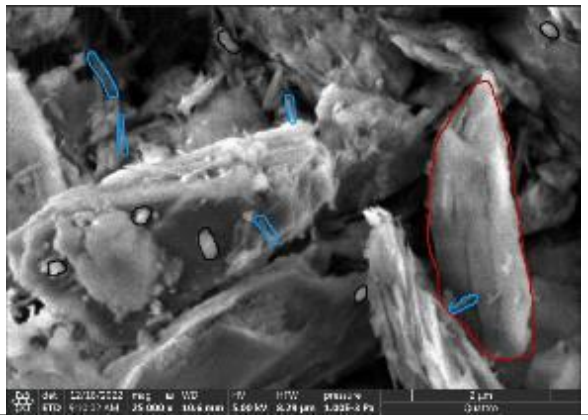

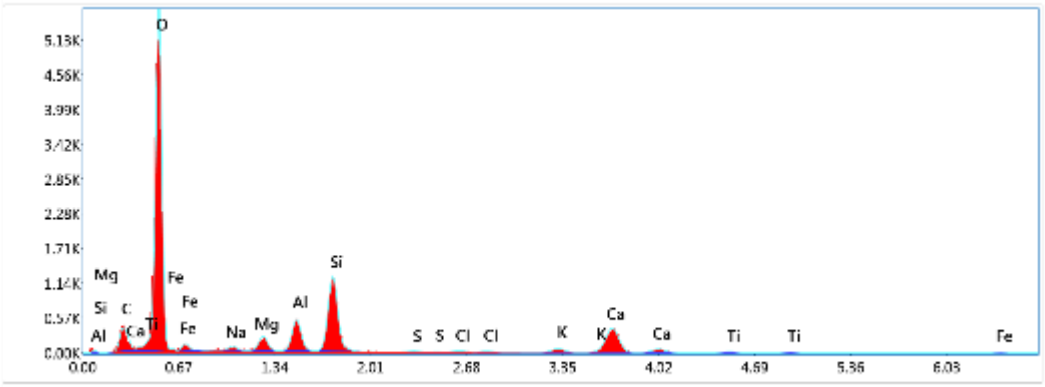
O
Mg
Si
C
Al
Ca
Ti
Fe
Fe
Fe
Na
Mg
Al
Si
S
S
Cl
Cl
K
K
Ca
Ca
Ti
Ti
Fe
5.13K
4.56K
3.99K
3.42K
2.85K
2.28K
1.71K
1.14K
0.57K
0.00K
0.00
0.67
1.34
2.01
2.68
3.35
4.02
4.69
5.36
6.03

(c)

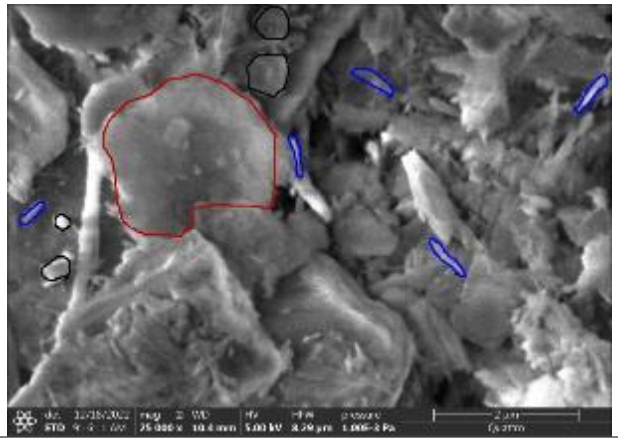

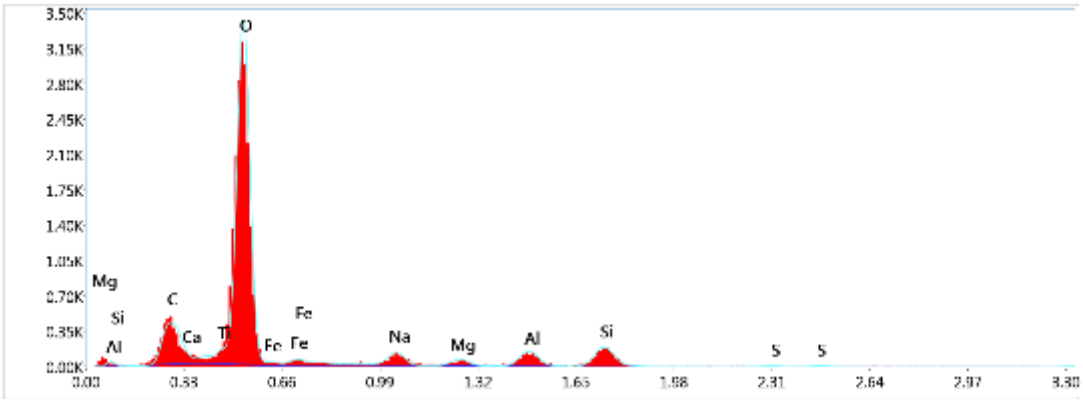

(d)

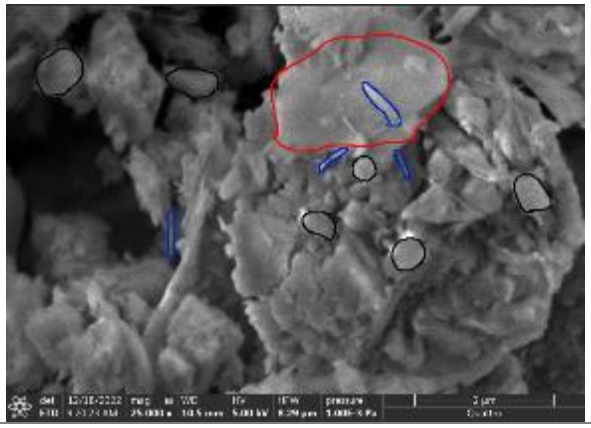

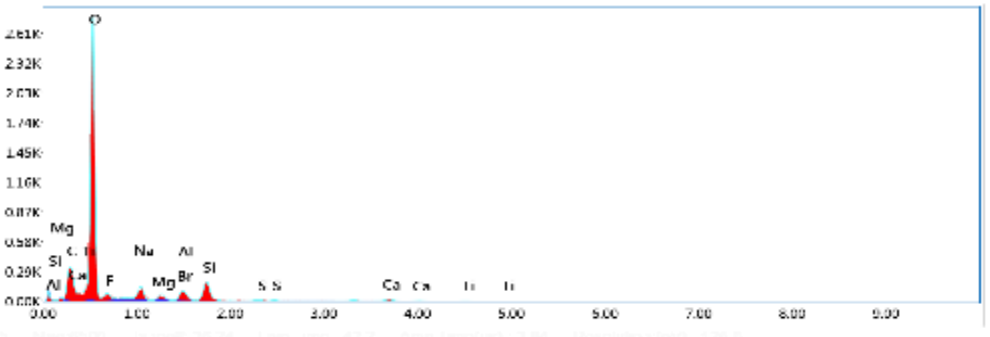

Figure 18 - SEM micrographs and SEM-EDX spectra (a) Tuff , (b) TuffMKGPM 8mole , (c) TuffMKGPM 10mole , (d) TuffMKGPM 12mole

4. Conclusions

The present study investigates the impact of adding metakaolin geopolymer cement as a binder on the mechanical and microstructural properties of tuff intended for road base layers. Based on the data presented, the following conclusions can be drawn:

- The results of this study demonstrate the potential of metakaolin geopolymer cement as a binder in tuff to improve its dry density. The increase in dry density can lead to improved mechanical properties, making tuff more suitable for load-bearing structures.
- The direct shear test indicates that the shear strength parameters of the TTG samples were notably superior to those of the UT samples. The highest values for cohesion and friction angle were observed in the TTG with a concentration of 12 moles of NaOH.
- The microstructural analysis suggests that the TuffMKGPM with 10 moles of alkaline activator is the optimal formulation, providing a dense and homogenous microstructure with minimal residual crystalline phases and voids. This molar ratio is likely to offer the best mechanical properties and durability, making it the preferred choice for sustainable construction applications.
- The 12mole mixture, despite its high strength, is not recommended due to potential durability issues. Therefore, the 10mole mixture is recommended for use in pavement base layers. Future research should explore long-term durability and environmental impacts to further validate these findings.

Acknowledgement

The authors would like to express their gratitude to the DGRSDT and ATRST for funding this research. Special thanks are also extended to the LTPO laboratory and the Laboratory of Technology at Tahri Mohammed University Bechar, Algeria, where the majority of this work was conducted. Additionally, appreciation goes to (PTAPC) CRAPC, Laghouat, Algeria for their assistance with microstructure analysis.

References

ALLALI, K., BELLA, N., & MEKKAOUI, A. (2024). Kaolin Valorisation as a Raw Material of Geopolymer Cement for Road Pavement Construction Used for Stabilizing Untreated Gravel. *Tobacco Regulatory Science (TRS)*, 1834–1861.

Amran, M., Al-Fakih, A., Chu, S. H., Fediuk, R., Haruna, S., Azevedo, A., & Vatin, N. (2021). Long-term durability properties of geopolymer concrete: An in-depth review. *Case Studies in Construction Materials*, *15*(July), e00661. https://doi.org/10.1016/j.cscm.2021.e00661

AMRAOUI, B., HOUMADI, Y., & MAMOUNE, S. M.-A. (2022). Elaboration of the geotechnical map of ain temouchent-city (Algeria). *Modelling in Civil Environmental Engineering*, *17*(2), 13–24. https://doi.org/10.2478/mmce-2022-0007

Avirneni, D., Peddinti, P. R. T., & Saride, S. (2016). Durability and long term performance of geopolymer stabilized reclaimed asphalt pavement base courses. *Construction and Building Materials*, *121*, 198–209. https://doi.org/10.1016/j.conbuildmat.2016.05.162

Bahaadin Noory Zangana, D. (2012). The Effect Of Sodium Hydroxide On The Strength Of Kirkuk Soil – Cement Mixtures. *Anbar Journal of Engineering Sciences*, *5*(2), 258–270.

https://doi.org/10.37649/aengs.2012.69038

Boukoffa, M., Lamouri, B., Bouabsa, L., & Fagel, N. (2021). *Characterization of Three Kaolinitic Clays (Ne Algeria): Comparative Study*. 1–28.

CEBTP. (1984). Guide pratique de dimensionnement des chausse´es pour lespays tropicaux.

Chen, K., Wu, D., Yi, M., Cai, Q., & Zhang, Z. (2021). Mechanical and durability properties of metakaolin blended with slag geopolymer mortars used for pavement repair. *Construction and Building Materials*, *281*, 122566. https://doi.org/10.1016/j.conbuildmat.2021.122566

Daheur, E. G., Taibi, S., Goual, I., & Li, Z. Sen. (2021). Hydro-mechanical behavior from small strain to failure of tuffs amended with dune sand – Application to pavements design in Saharan areas. *Construction and Building Materials*, *272*, 121948. https://doi.org/10.1016/j.conbuildmat.2020.121948

Faraldos, M., & Bahamonde, A. (2018). Multifunctional photocatalytic coatings for construction materials. In *Nanotechnology in Eco-efficient Construction: Materials, Processes and Applications*. Elsevier Ltd. https://doi.org/10.1016/B978-0-08-102641-0.00023-2

Gautam, P. K., Kalla, P., Jethoo, A. S., Agrawal, R., & Singh, H. (2018). Sustainable use of waste in flexible pavement: A review. *Construction and Building Materials*, *180*, 239–253. https://doi.org/10.1016/j.conbuildmat.2018.04.067

Germinario, L., & Török, Á. (2019). Variability of technical properties and durability in volcanic tuffs from the same quarry region – examples from Northern Hungary. *Engineering Geology*, *262*. https://doi.org/10.1016/j.enggeo.2019.105319

GTR -Guide des Terrassements Routiers- (2000). Réalisation des remblais et des couches de forme (GTR), Guide technique, 102 p., fascicules I et II, références SETRA: D9233-1 et D9233-2), SETRA- LCPC, 2ème édition, juillet 2000

Hamid, W., & Alnuaim, A. (2023). Sustainable geopolymerization approach to stabilize sabkha soil. *Journal of Materials Research and Technology*, *24*, 9030–9044. https://doi.org/10.1016/j.jmrt.2023.05.149

Hamzaoui, R., Muslim, F., Bennabi, A., & Guillin, J. (2015). *Structural and thermal behavior of proclay kaolinite using high energy ball milling process*. *271*, 228–237.

Hu, W., Nie, Q., Huang, B., Su, A., Du, Y., Shu, X., & He, Q. (2018). Mechanical property and microstructure characteristics of geopolymer stabilized aggregate base. *Construction and Building Materials*, *191*, 1120–1127. https://doi.org/10.1016/j.conbuildmat.2018.10.081

Jiang, W., Huang, Y., & Sha, A. (2018). A review of eco-friendly functional road materials. *Construction and Building Materials*, *191*, 1082–1092. https://doi.org/10.1016/j.conbuildmat.2018.10.082

Kamal, I., & Bas, Y. (2021). Materials and technologies in road pavements - An overview. *Materials Today: Proceedings*, *42*, 2660–2667. https://doi.org/10.1016/j.matpr.2020.12.643

Kamath, M., Prashant, S., & Kumar, M. (2021). Micro-characterisation of alkali activated paste with fly ash-GGBS-metakaolin binder system with ambient setting characteristics. *Construction and Building Materials*, *277*, 122323. https://doi.org/10.1016/j.conbuildmat.2021.122323

Kantarci, F., Türkmen, İ., & Ekinci, E. (2021). Improving elevated temperature performance of

geopolymer concrete utilizing nano-silica, micro-silica and styrene-butadiene latex. *Construction and Building Materials*, *286*. https://doi.org/10.1016/j.conbuildmat.2021.122980

Kantarcı, F., Türkmen, İ., & Ekinci, E. (2019). Optimization of production parameters of geopolymer mortar and concrete: A comprehensive experimental study. *Construction and Building Materials*, *228*. https://doi.org/10.1016/j.conbuildmat.2019.116770

Khalifa, A. Z., Cizer, Ö., Pontikes, Y., Heath, A., Patureau, P., Bernal, S. A., & Marsh, A. T. M. (2020). Cement and Concrete Research Advances in alkali-activation of clay minerals. *Cement and Concrete Research*, *132*(March), 106050. https://doi.org/10.1016/j.cemconres.2020.106050

Levitskii, I. A., Pozniak, A. I., & Baranceva, S. E. (2013). Effects of the Basaltic Tuff Additions on the Properties , Structure and Phase Composition of the Ceramic Tiles for Interior Wall Facing. *Procedia Engineering*, *57*, 707–713. https://doi.org/10.1016/j.proeng.2013.04.089

Liu, S. H., Sun, D., & Matsuoka, H. (2005). On the interface friction in direct shear test. *Computers and Geotechnics*, *32*(5), 317–325. https://doi.org/10.1016/j.compgeo.2005.05.002

Majd, M. T., Davoudi, M., Ramezanzadeh, M., Ghasemi, E., Ramezanzadeh, B., & Mahdavian, M. (2020). Construction of a smart active/barrier anti-corrosion system based on epoxy-ester/zinc intercalated kaolin nanocontainer for steel substrate. *Construction and Building Materials*, *247*, 118555. https://doi.org/10.1016/j.conbuildmat.2020.118555

Nabbou, N., Belhachemi, M., Boumelik, M., Merzougui, T., Lahcene, D., Harek, Y., Zorpas, A. A., & Jeguirim, M. (2019). Removal of fluoride from groundwater using natural clay (kaolinite): Optimization of adsorption conditions. *Comptes Rendus Chimie*, *22*(2–3), 105–112. https://doi.org/10.1016/j.crci.2018.09.010

Okoye, F. N. (2017). Geopolymer binder: A veritable alternative to Portland cement. *Materials Today: Proceedings*, *4*(4), 5599–5604. https://doi.org/10.1016/j.matpr.2017.06.017

Plati, C. (2019). Sustainability factors in pavement materials, design, and preservation strategies: A literature review. *Construction and Building Materials*, *211*, 539–555. https://doi.org/10.1016/j.conbuildmat.2019.03.242

Polini, A., & Yang, F. (2017). Physicochemical characterization of nanofiber composites. In *Nanofiber Composites for Biomedical Applications*. Elsevier Ltd. https://doi.org/10.1016/B978-0-08-100173-8.00005-3

Rikioui, T., Lebaili, S., & Tafraoui, A. (2021). *Valorization of local kaolin in sustainable concrete and on the environment through their exploitation deposit*. *April*. https://doi.org/10.37789/rjce.2021.12.1.7

Sahnoune, F., Chegaar, M., Saheb, N., Goeuriot, P., & Valdivieso, F. (2008). Algerian kaolinite used for mullite formation. *Applied Clay Science*, *38*(3–4), 304–310. https://doi.org/10.1016/j.clay.2007.04.013

Singh, B., Ishwarya, G., Gupta, M., & Bhattacharyya, S. K. (2015). Geopolymer concrete: A review of some recent developments. *Construction and Building Materials*, *85*, 78–90. https://doi.org/10.1016/j.conbuildmat.2015.03.036

Singh, N. B., & Middendorf, B. (2020). Geopolymers as an alternative to Portland cement: An overview. *Construction and Building Materials*, *237*, 117455.

https://doi.org/10.1016/j.conbuildmat.2019.117455

Tang, Z., Li, W., Hu, Y., Zhou, J. L., & Tam, V. W. Y. (2019). Review on designs and properties of multifunctional alkali-activated materials (AAMs). *Construction and Building Materials*, *200*, 474–489. https://doi.org/10.1016/j.conbuildmat.2018.12.157

Thiha, S., Lertsuriyakul, C., & Phueakphum, D. (2018). *SHEAR STRENGTH ENHANCEMENT OF COMPACTED SOILS USING HIGH-CALCIUM FLY ASH-BASED GEOPOLYMER*. *15*(48), 1–9.

Tiago, I., & Gil, F. (2020). *International Biodeterioration & Biodegradation In vitro analyses of fungi and dolomitic limestone interactions : Bioreceptivity and biodeterioration assessment Jo a*. *155*(July). https://doi.org/10.1016/j.ibiod.2020.105107

Wang, S., & Mulligan, C. N. (2006). *Natural attenuation processes for remediation of arsenic contaminated soils and groundwater*. *138*, 459–470. https://doi.org/10.1016/j.jhazmat.2006.09.048

Yu, Z., Zhang, T., Deng, Y., Han, Y., Zhang, T., Hou, P., & Zhang, G. (2023). Microstructure and mechanical performance of alkali-activated tuff-based binders. *Cement and Concrete Composites*, *139*(December 2022), 105030. https://doi.org/10.1016/j.cemconcomp.2023.105030

Zenasni, M. A., Meroufel, B., Merlin, A., & George, B. (2014). Adsorption of Congo Red from Aqueous Solution Using CTAB-Kaolin from Bechar Algeria. *Journal of Surface Engineered Materials and Advanced Technology*, *04*(06), 332–341. https://doi.org/10.4236/jsemat.2014.46037